

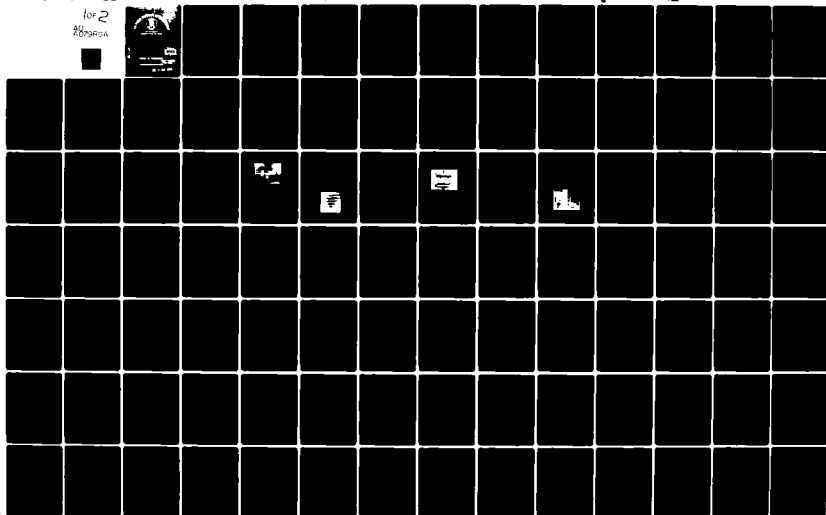
AD-A079 854

AIR FORCE INST OF TECH WRIGHT-PATTERSON AFB OH SCHOO--ETC F/G 20/11
AN EXPERIMENTAL WEIGHT FUNCTION METHOD FOR STRESS INTENSITY FAC--ETC(U)
DEC 79 D BAR-TIKVA
AFIT/6AE/AA/79D-2

UNCLASSIFIED

NL

for 2
pages



ADA 079854



14

AFIT/GAE/AA/79D-2

ADA 079854

940666-1

6

AN EXPERIMENTAL WEIGHT FUNCTION
METHOD FOR STRESS INTENSITY
FACTOR CALIBRATION,

THESIS

AFIT/GAE/AA/79D-2

16

Dan Bar-Tikva
Major IAF

DDC
RECEIVED
JAN 28 1980
A

DDC FILE COPY

11/1/79
1110

Approved for public release; distribution unlimited

013,225

y/3

AN EXPERIMENTAL WEIGHT FUNCTION
METHOD FOR STRESS INTENSITY
FACTOR CALIBRATION

THESIS

Presented to the Faculty of the School of Engineering
of the Air Force Institute of Technology

Air University

in Partial Fulfillment of the
Requirements for the Degree of
Master of Science

By

Dan Bar-Tikva, B.S.

Major IAF

Graduate Aeronautical Engineering

Accession For	
NTIS GRA&I	<input checked="checked" type="checkbox"/>
DEC TAB	<input type="checkbox"/>
Unannounced	<input type="checkbox"/>
Justification	
By	
Date	
Approved	
Initials	Signature

December 1979

Approved for public release; distribution unlimited

Preface

The work that led to this report was conducted at the Air Force Material Laboratories (AFML) at Wright-Patterson Air Force Base (WPAFB), and sponsored by AFML/LLN. It combines a laser interferometry technique that has been developed at the AFML with the weight function idea to demonstrate a complete experimental way to find stress intensity factors for a certain cracked body without the need to load the body with the actual load of interest, but rather with any other loading configuration that one might find easy to apply.

At this opportunity I would like to express my gratitude to my thesis advisor, Dr. A. F. Grandt, Jr., for his inspiring guidance. I would also wish to thank Professor A. Palazotto for his advise and fruitful suggestions during the course of this work.

A special thanks I owe to Dr. T. Nicholas and the staff of engineers and technicians in AFML/Metal and Ceramics Division/Metal Behavior Branch (LLN), for permission to use the fracture mechanic laboratories and the remarkable assistance and advice during this project. Without their help I would not be able to conclude this work.

I deeply thank my wife, Rachel, for the encouragement, patience and understanding she showed me during the time of this study.

— Dan Bar-Tikva

Contents

	Page
Preface	ii
List of Figures	v
List of Tables	vii
List of Symbols	viii
Abstract	xi
I. Introduction	1
Background	1
Purpose	3
General Approach	3
II. Theory	5
General Assumptions	5
Stress Intensity Factor	5
The Weight Function	7
K Calibration by Crack Tip Displacement	11
Crack Opening Calibration	13
K_I For Case 2	16
III. Experimental Technique	17
The Laser Interferometry Method	17
Test Apparatus	20
Test Procedure	24
IV. Data Reduction and Numerical Technique	26
K_I For Case 1	26
Crack Mouth Opening	27
Numerical Technique for K_I Case 2 Computation	27
V. Experimental Results	30
Experimental Measurements	30
Data Interpolation	31
Crack Profile Measurements	38

	Page
Case 2 Loadings	38
Uniform Tension	38
Three Point Bending	43
VI. Conclusions	52
Bibliography	54
Appendix A: The Weight Function	57
Appendix B: Justification of Assumptions	62
Appendix C: Laser Interferometer Data Reduction	65
Appendix D: Computer Program Description	69
Appendix E: Crack Shape--Conical Approximation	90
Vita	95

List of Figures

Figure		Page
2.1	Crack Opening Modes	6
2.2	Crack Tip Stress Coordinates	7
2.3	Cracked Body Loading Configuration	8
2.4	Superposition	9
2.5	Edge Crack	14
3.1	Surface Indentation	18
3.2	Schematic Showing Fringe Pattern Generation . .	19
3.3	Typical Interference Fringe Pattern	19
3.4	Test Specimen	20
3.5	Specimen Set Up in Bending Fixture	21
3.6	Clip Gage Setup	22
3.7	Laser Beam Reflection	23
3.8	Test Apparatus Setup	23
5.1	Specimen Dimensions	30
5.2	Loading Fixture Dimension	31
5.3	Stress Intensity Factor (Nondimensional) for Pure Bending	36
5.4	Crack Mouth Opening (Nondimensional) for Pure Bending	37
5.5	Nondimensional Displacement Along Crack Surface Compared to Orange Equation (Ref 11) Pure Bending $a/W=0.436$	39
5.6	Nondimensional Displacements Along Crack Surface Compared to Orange Equation (Ref 11) Pure Bending, $a/W=0.7517$	40

Figure		Page
5.7	Case 2 Loading Configurations	41
5.8	Stress Intensity Factor (Nondimensional) for Uniform Tension	44
5.9	A Uniform Strip Under Three-Point Bending . . .	45
5.10	Stress Intensity Factor (Nondimensional) for Three-Point Bending $S/W=4$	50
5.11	Stress Intensity Factor (Nondimensional) for Three-Point Bending, $S/W=8$	51
A.1	Loaded Cracked Body	57
B.1	Irwin Circular Plastic Zone Model	62
C.1	Typical Stripchart Recorder Trace of Fringe Motion, Load and Crack Mouth Opening	66
C.2	Typical Load-Fringe Motion Curve	68
E.1	Crack Opening Conical Approximation	90

List of Tables

Table		Page
I	Experimental Measurement Results	32
II	K_I (Nondimensional) Comparison of Actual Data to Interpolated Data	34
III	η_o (Nondimensional) Comparison of Actual Data to Interpolated Data	35
IV	K_I (Nondimensional) for Uniform Tension . . .	42
V	K_I (Nondimensional) for Three-Point Bending, $S/W=4$	48
VI	K_I (Nondimensional) for Three-Point Bending, $S/W=8$	49
C.I	Fringe Order Versus Load	67

List of Symbols

A	Area
a	Crack length
B	Coefficient defined by Eq (2-23)
b	Material thickness
C	Compliance
c	Half the height of the beam W/2
d	Distance between indentation
E	Young elastic modulus
f	Body forces
G	Shear modulus
\dot{g}	Griffith energy release rate
H	$\left\{ \begin{array}{l} E \quad \text{plane stress} \\ \frac{E}{1-\nu^2} \quad \text{plane strain} \end{array} \right.$
h	Weight function
i,j,n	Indices
K	Stress intensity factor
\bar{K}	Curvature
K_I	Mode I stress intensity factor
\bar{K}_I	Nondimensional mode I stress intensity factor
K_{II}	Mode II stress intensity factor
K_{III}	Mode III stress intensity factor
K_{IC}	Mode I fracture toughness
k	Stress intensity factor per unit load

ℓ	Half span between supports
M	Moment
m	Fringe order
\bar{m}	Orange conic section coefficient
p	Crack surface tractions
P	Load
R	Coefficient defined by Eq (2-24)
\bar{R}	Radius of curvature
r	Radius from crack tip
r_p	Plastic zone radius
S	Span between supports
s	Path
T	Surface tractions
t	Coordinate along crack, starting at the crack tip
U	Total strain energy stored in the cracked body
u_i^m	Displacement at location i for load P_m
u_x	Displacement in x direction
u_y	Displacement in y direction
W	Beam or strip height
x, y	Cartesian coordinate
Y	Nondimensional stress intensity factor
α_o	Diffraction angle
Γ	Path
δd	Change in distance between indentations
δm	Change in fringe order
ϵ	Strain

η	Crack surface vertical displacement
η_0	Crack mouth vertical displacement
λ	Wave length
θ	Angular coordinate
ν	Poisson ratio
σ_{ij}	Stress components
$\sigma_{y.s}$	Yield stress

Abstract

The weight function procedure allows one to convert stress intensity factors K and crack displacement information obtained for one crack configuration and loading into the stress intensity factor solution for the same geometry and another loading.

The feasibility of using the weight function idea for a two-dimensional case with experimental results is demonstrated in this work. Mode I stress intensity factor K_I measurements obtained by a laser interferometric technique, and "crack mouth" opening displacement measurements were taken for an edge cracked strip subjected to four-point bending. These results were used to construct (numerically) a weight function with the aid of a computer program written for this purpose.

Results of K_I for the same geometry with two different loading configurations, uniform tension and three-point bending (with two different length to width ratios) were computed.

These results agree favorably with the known solutions and demonstrate that a set of experiments for a single loading can accurately predict the stress intensity factor for any other loading configuration of the same geometry. The advantage of the weight function method would be particularly important if these loading configurations are difficult or impossible to reproduce in the laboratory.

AN EXPERIMENTAL WEIGHT FUNCTION METHOD FOR STRESS INTENSITY FACTOR CALIBRATION

I. Introduction

Background

Fracture mechanics presently provides the best available tools to quantitatively assess the influence of preexistent cracks in structures. Although fracture mechanics, as we now know it, is a relatively new technology (since the mid 1950s), the basic ideas were already presented by Griffith (Ref 1) in the early 1920s.

Current linear elastic fracture mechanics (LEFM) concepts assume that the stress intensity factor K , the parameter that relates load, crack length and geometry controls fracture ($K = K_C = \text{constant at fracture}$) and crack propagation (Ref 23).

Stress intensity factor calibrations are required for any fracture or crack propagation analysis. Since crack tip analysis can be complex, experimental K solutions often become necessary to verify or supplement analytical or numerical solutions.

For complex type geometries and loading configurations which commonly exist in aircraft structures, experimentation may be the primary method to obtain a reasonably

accurate and dependable solution. Conducting experiments on actual parts and loadings is often a very difficult and costly procedure.

The main motivation for this thesis investigation was to find a technique that may, in some cases, greatly reduce the experimental effort required in order to obtain a K solution.

An analytical approach to determine the stress intensity factors K was discussed by Bueckner (Ref 2) and Rice (Ref 3). They showed that once the displacement field and stress intensity factors are known for one geometry and loading configuration referred to subsequently as Case 1, K may be obtained for any other loading (Case 2) applied to the same crack geometry (Refs 4-8, 21). The method depends mainly on the reciprocal theorem and strain energy expressions. A load and material independent weight function can be constructed to relate the stress intensity factor, material properties, and crack length together with crack surface opening (for more details see Part II and Appendix A).

The significant advantage of this procedures lies in the fact that only the first problem (Case 1) needs to be solved directly. Construction of the weight function for this case allows ready determination of K for any other loading on the same crack geometry (Cases 2, 3, etc.). Stress intensity factors may then be obtained for a variety of other specimen loadings some of which may be highly complex compared to the original. In addition, the

computational expenses are minimal because only a single relatively simple load configuration needs to be calculated.

The only additional information required for any other case is the stress distribution at the crack location for a noncracked body under the load configuration in question. This stress distribution is available, in many cases, from the static crack free stress analysis or can be obtained with much less effort than a cracked body analysis requires.

Purpose

Although weight functions have been employed with analytical, finite elements and other numerical methods, the author is unaware of attempts to combine weight functions with experimental procedures.

The objective of this work was to show that the weight function idea can assist the experimentalist by allowing him an opportunity to obtain the stress intensity factor solution for a complex loading configuration from the results of a simple experiment, and also to obtain K solutions for a variety of loadings from a single set of experiments. This will greatly reduce the complexity and scope of the experimental effort.

General Approach

The weight function procedure is demonstrated with experimental results for an edge crack specimen.

The reference (Case 1) problem has been chosen as an edge cracked strip subjected to four-point bending. Crack surface displacement measurements near the crack tip were obtained by a laser interferometric method following the technique developed at the Air Force Materials Laboratory (Refs 9, 10, 19). These results gave the mode I stress intensity factor K_I for that case. Crack mouth opening measurements, using a clip gage, were then used to construct the crack surface displacement function incorporating Orange (Ref 11) conic section approximation. These experimental results were used to evaluate the weight function and predict the stress intensity factor K_I for other cases, which were chosen to be uniform tension and three-point bending. The results were compared with the known solution given in (Refs 12-14).

II. Theory

General Assumptions

1. Linear elastic fracture mechanics (LEFM) applies i.e., the amount of plasticity near the crack tip is relatively small

$$\frac{r_p}{a} \leq 0.1$$

where r_p is the radius of plastic zone. (See Hertzberg, Ref 15, and Appendix B for a more detailed discussion.)

2. The problem is assumed to be purely two-dimensional; i.e., no variations through the thickness are considered.

3. Body forces are assumed to be negligible.

4. Only pure Mode I crack openings will be discussed.

Stress Intensity Factor

The stress intensity factor K is the linear elastic fracture mechanic (LEFM) parameter that relates load, crack length and geometry. The LEFM approach to predicting crack growth assumes that K controls:

1. Fracture ($K = K_C = \text{constant at fracture}$).
2. Crack propagation due to fatigue.
3. Crack propagation due to stress corrosion.

Three modes of stress intensity factors are defined depending on the crack tip opening mode (Fig. 2.1). They may be stated as:

$$\text{Mode I Opening } K_I = \lim_{r \rightarrow 0} \sqrt{2\pi r} \sigma_y \quad (\theta=0) \quad (2-1)$$

$$\text{Mode II Sliding } K_{II} = \lim_{r \rightarrow 0} \sqrt{2\pi r} \sigma_{xy} \quad (\theta=0) \quad (2-2)$$

$$\text{Mode III Tearing } K_{III} = \lim_{r \rightarrow 0} \sqrt{2\pi r} \sigma_{yz} \quad (\theta=0) \quad (2-3)$$

where crack tip coordinates are defined in Fig. 2.2

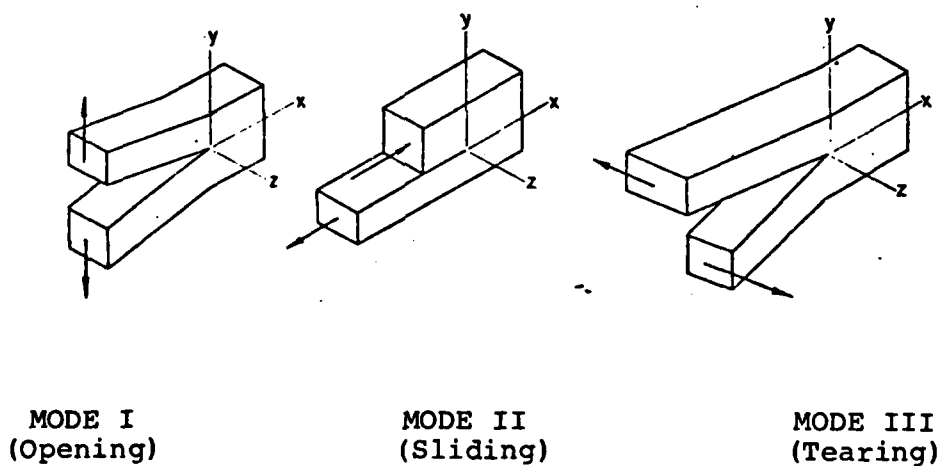


Fig. 2.1. Crack Opening Modes

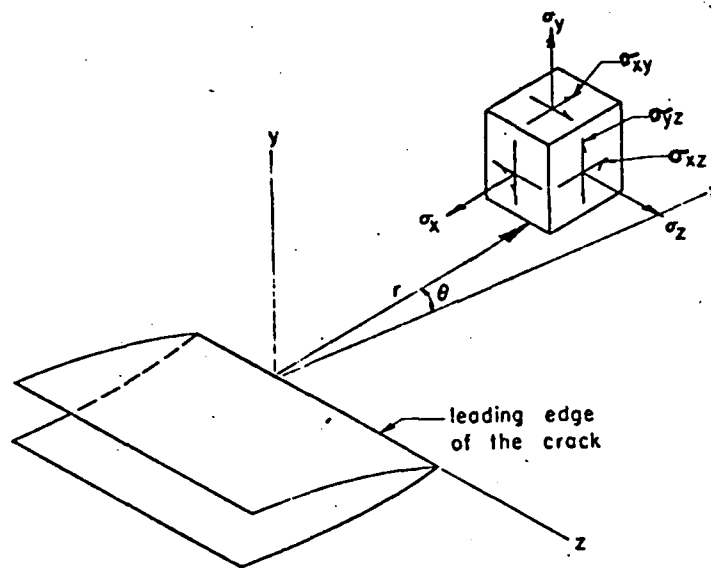


Fig. 2.2. Crack Tip Stress Coordinates

This work deals only with the opening Mode I, though it can be easily extended to other "modes."

The Weight Function

The Mode I stress intensity factor K_I under arbitrary loading, shown in Fig. 2.3, can be given as:

$$K_I = \int_{\Gamma} T \cdot h d\Gamma + \int_A f \cdot h \cdot dA \quad (2-4)$$

(see Appendix A and Refs 2-6 for detailed discussion).

where:

Γ is any path chosen around the body that includes all the surface tractions and body forces,

A is the region defined by Γ ,

T designates surface tractions,

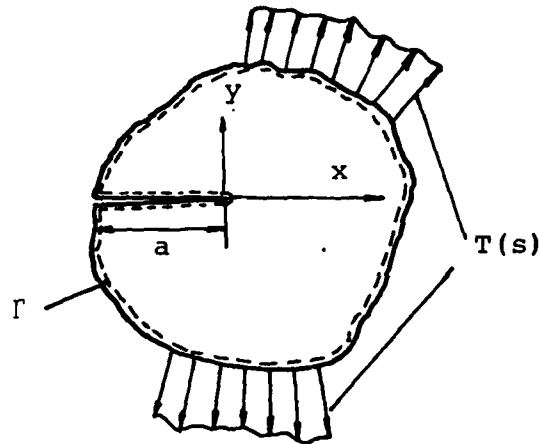


Fig. 2.3. Cracked Body Loading Configuration

K_I is the Mode I stress intensity solution corresponding to the loads T and f ,

f are body forces,

$$h = h(x, y, a) = \frac{H}{2K_I} \frac{\partial \eta(x, y, a)}{\partial a} \quad (\text{the weight function}) \quad (2-5)$$

$\eta(x, y, a)$ is the crack vertical displacement for any chosen load configuration (independent of T and f),

K_I in the weight function, Eq (2-5), is the Mode I stress intensity solution that corresponds to the η solution, and

$$H = \begin{cases} E & \text{for plane stress} \\ \frac{E}{1-\nu^2} & \text{for plane strain.} \end{cases}$$

The weight function h is independent of the loads T , f and material properties and can be calculated for the same geometry from another known solution of K_I and $\partial \eta / \partial a$.

Using the principle of superposition of linear elasticity, the calculations of the stress intensity factor

considering the case of a cracked body under a certain loading configuration is equal to the case of the cracked body where only the crack surface is subjected to tractions $p(x)$ (coordinates are chosen so that the crack is in x direction). Here $p(x)$ is the stress σ_y that will occur at the crack location for an uncracked body subjected to the original loading configuration. This idea is demonstrated in Fig. 2.4.

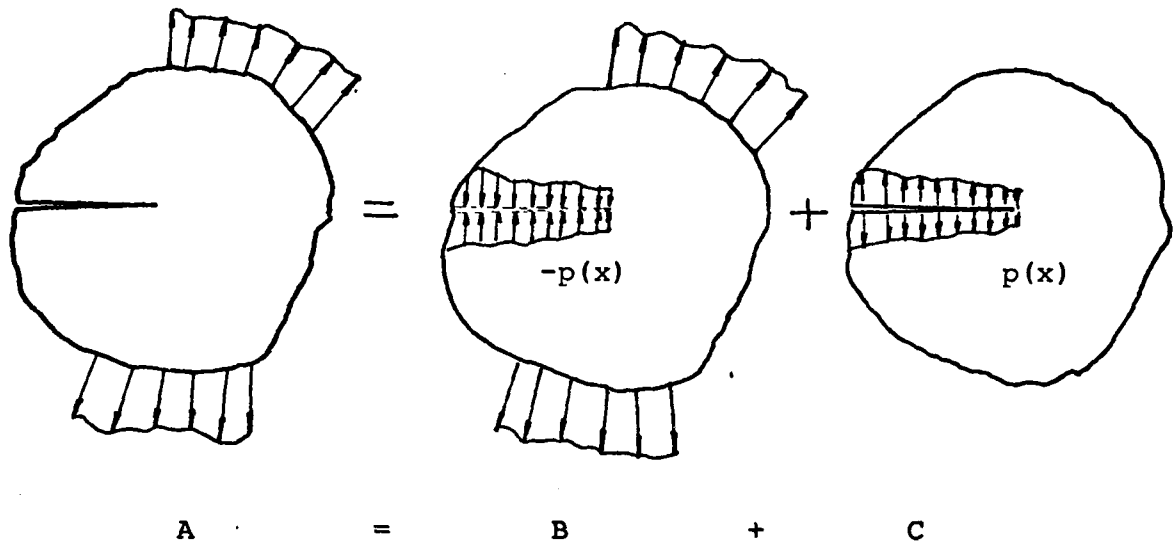


Fig. 2.4. Superposition

$$K_I \textcircled{A} = K_I \textcircled{B} + K_I \textcircled{C}$$

Part B can be viewed as a noncracked body; therefore,

$$K_I \textcircled{B} = 0 \Rightarrow K_I \textcircled{A} = K_I \textcircled{C}$$

If one chooses the path Γ as any path that includes the crack surface and, for simplicity, takes a straight crack in the x-direction as in Fig. 2.4 (the last assumption is not essential and is used only to simplify the equations), then the Eq (2-4) for K_I can be stated as:

$$K_I = \int_0^a h(x,a)p(x)dx - \int_a^0 h(x,a)p(x)dx \quad (2-6)$$

Reversing the integration limits and adding the two integrals we get:

$$K_I = 2 \int_0^a h(x,a)p(x)dx \quad (2-7)$$

The unknown stress intensity solution for the loading $p(x)$ is considered Case 2, and the known solution, from which the weight function will be computed, is taken as Case 1, then Eq (2-7) can be written as

$$K_{I\text{ } \textcircled{2}} = 2 \int_0^a h_{\textcircled{1}}(x,a)p_{\textcircled{2}}(x)dx \quad (2-8)$$

and from Eq (2-5)

$$h_{\textcircled{1}}(x,a) = \frac{H}{2K_{I\text{ } \textcircled{1}}} \left(\frac{\partial \eta(x,a)}{\partial a} \right)_{\textcircled{1}} \quad (2-9)$$

If Eq (2-9) is substituted into Eq (2-8), the result is:

$$K_{I(2)} = \frac{H}{K_{I(1)}} \int_0^a p(x)_{(2)} \left(\frac{\partial \eta(x, a)}{a} \right)_{(1)} dx \quad (2-10)$$

where

$K_{I(2)}$ is the Mode I stress intensity factor to be found,

$p(x)_{(2)}$ is the stress σ_y at the crack location for a noncracked body with loading configuration of Case 2,

$K_{I(1)}$ is the Mode I stress intensity factor for Case 1 and will be determined experimentally, and

$\frac{\partial \eta}{\partial a}_{(1)}$ is the derivative with respect to crack length of the crack opening profile for Case 1. η is also determined experimentally.

K Calibration by Crack Tip Displacement

The crack tip displacement field is defined by the following relations that represent the elasticity solution for the stress-displacement field in terms of K near the crack tip of a cracked body. One can take these displacement expressions for Mode I opening (Refs 17, 18, 10) as:

$$u_x = \frac{K_I}{G} \sqrt{\frac{r}{2\pi}} \cos \frac{\theta}{2} \left[\frac{1-\nu}{1+\nu} + \sin^2 \frac{\theta}{2} \right] \quad (2-11)$$

$$u_y = \frac{K_I}{G} \sqrt{\frac{r}{2\pi}} \sin \frac{\theta}{2} \left[\frac{2}{1+\nu} - \cos^2 \frac{\theta}{2} \right] \quad (2-12)$$

for plane stress; and

$$u_x = \frac{K_I}{G} \sqrt{\frac{r}{2\pi}} \cos \frac{\theta}{2} \left[1-2\nu + \sin^2 \frac{\theta}{2} \right] \quad (2-13)$$

$$u_y = \frac{K_I}{G} \sqrt{\frac{r}{2\pi}} \sin \frac{\theta}{2} \left[2-2\nu - \cos^2 \frac{\theta}{2} \right] \quad (2-14)$$

for plane strain.

Consider the vertical displacement u_y along the crack surface for which

$$\theta = \pi$$

$$r = t$$

where t is a coordinate along the crack, starting at the crack tip. One should note to conform with usual practice, η replaces the displacement in y direction u_y . Recall from elasticity that:

$$G = \frac{E}{2(1+\nu)} \quad (2-15)$$

Substituting into Eqs (2-12) and (2-14) the crack displacement for plane stress and plane strain can be written as

$$\eta = \frac{4K_I}{H} \left(\frac{t}{2\pi} \right)^{\frac{1}{2}} \quad (2-16)$$

$$K_I = \frac{\eta H}{4} \left(\frac{2\pi}{t} \right)^{\frac{1}{2}} \quad (2-17)$$

The equation holds only very near the crack tip

$$t \ll a$$

and allows one to calibrate K_I by measuring crack opening at a known distance very near the crack tip.

Crack Opening Calibration

In order to find the slope with respect to the crack length $\partial\eta/\partial a$ of the crack opening profile, an approximation has been used. Orange (Ref 11) suggested a conic section approximation for a finite width edge cracked plate. This approximation is based on assuming a general conic section function for the crack opening shape and fitting the crack tip radius of curvature and crack mouth opening to determine the unknown coefficients. Further development of this relationship is presented in Appendix E. Following Orange and substituting for the crack tip curvature in terms of the stress intensity factor, using crack tip displacement equations, the following expression is derived:

$$\left(\frac{\eta}{\eta_o}\right)^2 = \frac{2}{2+\bar{m}} \left(\frac{t}{a}\right) + \frac{\bar{m}}{2+\bar{m}} \left(\frac{t}{a}\right)^2 \quad (2-18)$$

where η_o is the crack mouth displacement and \bar{m} is the conic section coefficient.

$$\bar{m} = \pi \left[\frac{H\eta_o}{2\sigma a Y} \right]^2 - 2 \quad (2-19)$$

Y is a nondimensional stress intensity factor

$$Y = \frac{K_I}{\sigma\sqrt{a}} \quad (2-20)$$

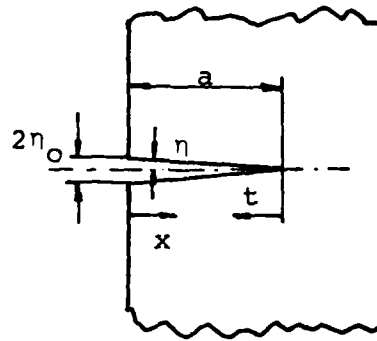


Fig. 2-5. Edge Crack

Crack displacements of finite single edged cracked strips under bending or tension generated by the Orange Eq (2-18) were compared to the collocation method presented by Gross (Ref 20) and found to match within 3.2 percent. The Orange equation was compared to the Rice (Ref 3) solution for a center crack considering an infinite plate. The results were found to be exactly the same. The Orange equation was also used successfully by Grandt (Refs 6, 21) for cracks in fastener holes and for radially cracked rings. Substituting the expression for Y Eq (2-20), and \bar{m} Eq (2-19) into Eq (2-18), we obtain

$$\left(\frac{\eta}{\eta_0}\right)^2 = \frac{2}{\pi \left[\frac{H\eta_0}{2a^{3/2}K_I} \right]^2} \left(\frac{t}{a}\right) + \left[1 - \frac{8aK_I^2}{\pi H^2 \eta_0^2} \right] \left(\frac{t}{a}\right)^2 \quad (2-21)$$

$$\eta^2 = \left[\frac{8K_I^2}{\pi H^2} \right] t + \left[\frac{\eta_0^2}{a^2} - \frac{8K_I^2}{\pi H^2 a} \right] t^2 \quad (2-22)$$

In order to simplify the above equation,

$$\text{let} \quad B = \frac{8K_I^2}{\pi H^2} \quad (2-23)$$

$$\text{and} \quad R = \frac{\eta_o^2}{a^2} - \frac{8K_I^2}{\pi H^2 a} \quad (2-24)$$

$$\text{Thus,} \quad \eta = [Bt + Rt^2]^{\frac{1}{2}} \quad (2-25)$$

$$\text{Also,} \quad \frac{\partial \eta}{\partial a} = \frac{1}{2} [Bt + Rt^2]^{-\frac{1}{2}} \cdot \frac{\partial}{\partial a} [Bt + Rt^2] \quad (2-26)$$

From Fig. 2.5, if $t = a - x$, then $\frac{\partial t}{\partial a} = 1$.

Thus,

$$\frac{\partial \eta}{\partial a} = \frac{1}{2} [Bt + Rt^2]^{-\frac{1}{2}} \left[\frac{\partial B}{\partial a} t + B + \frac{\partial R}{\partial a} t^2 + 2Rt \right] \quad (2-27)$$

where:

$$\frac{\partial B}{\partial a} = \frac{16K_I}{\pi H^2} \frac{\partial K_I}{\partial a} \quad (2-28)$$

and

$$\frac{\partial R}{\partial a} = \frac{8K_I^2}{\pi H^2 a^2} + \frac{2\eta_o}{a^2} \frac{\partial \eta_o}{\partial a} - \frac{2\eta_o^2}{a^3} - \frac{16K_I}{\pi H^2 a} \frac{\partial K_I}{\partial a} \quad (2-29)$$

Eq (2-27) therefore defines $\partial \eta / \partial a$ in terms of the crack mouth displacement η_o and the stress intensity factor K_I and their derivative with respect to the crack length.

K_I For Case 2

Substituting Eq (2-27) into Eq (2-10) and also changing the integration variable from x to t one obtains

$$K_{I(2)} = \frac{H}{2K_{I(1)}} \int_0^a p(t)_{(2)} [Bt + Rt^2]^{-\frac{1}{2}} [B + (\frac{\partial B}{\partial a} + 2R)t + \frac{\partial R}{\partial a} t^2] dt \quad (2-30)$$

where B , R , $\frac{\partial B}{\partial a}$ and $\frac{\partial R}{\partial a}$ are defined previously and calculated for Case 1.

From Eq (2-30) it is clear that measuring the stress intensity factor K_I and the crack mouth opening η_0 for various crack lengths and calculating their derivatives with respect to "a" allows one to construct the weight function for the Case 1 loading configuration. By knowing the stress distribution at the crack location for a non-cracked body under the loading configuration of Case 2 $p(t)_{(2)}$, one may obtain K_I for Case 2.

Computing this integral is quite tedious though possible for very simple forms of $p(t)$. However, numerical integration is possible for any $p(t)$ even if represented by a discrete numerical solution. In performing numerical integration, one should be cautioned to the fact that the weight function and therefore the whole expression under the integral is square root singular at the crack tip $t=0$ but still it can be shown that for the problems studied here a limit exists for the integral and, in most cases, the numerical integration converges quite rapidly.

III. Experimental Technique

The Laser Interferometry Method

Stress intensity factor K calibrations obtained by measuring crack tip displacements require a technique capable of accurately measuring extremely small displacements very near the crack tip. As a "rule of thumb" the relations for the crack tip displacement field as expressed in Eqs (2-11 to 2-14) are regarded to be sufficiently accurate within a distance of $a/20$ or smaller from the crack tip, where " a " is the crack length. The laser interferometry technique described here was reported in Refs 9, 10, and 19 to measure displacements of 0.1 microns at a distance of 50 microns from the crack tip.

Results were reported leading to K_I values that varied up to 15 percent from the theoretical value (for individual points). Most of these deviations were attributed to the imperfect crack and material characteristics and not to measurement errors. The technique is basically similar to conventional interferometry but only measures in-plane displacements on the surface.

Two small indentations are placed with a diamond indenter on both sides of the crack near the crack tip. Those indentations are typically square based pyramids with a base length of 20-40 microns and located 50 microns

apart on both sides of the crack (see Fig. 3.1).

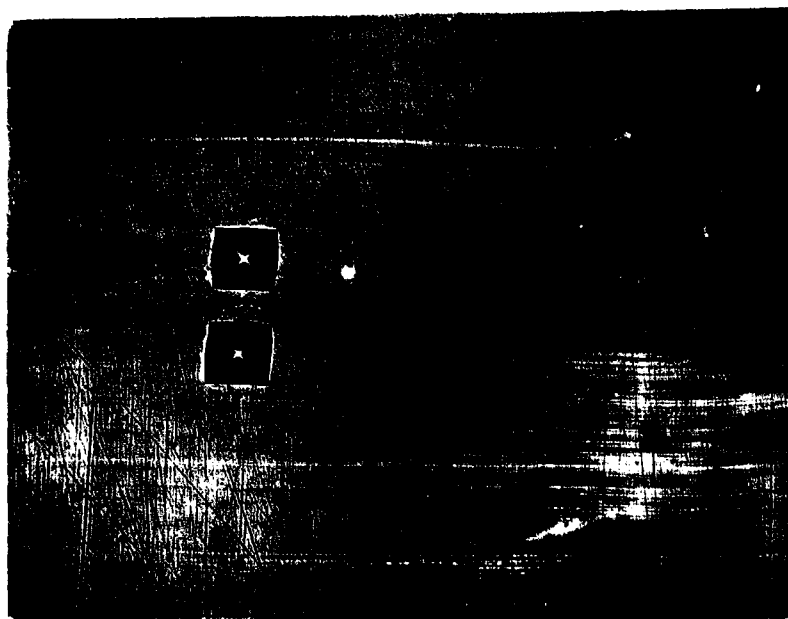


Fig. 3.1. Surface Indentation (x280 magnification)

A laser coherent source impinges upon the indentations. The beam is diffracted back at an angle α_0 with respect to the incident beam as shown schematically in Fig. 3.2.

Since the indentations are placed close together, the respective diffraction beam overlaps resulting in interference fringe patterns on either side of the incident laser beam. A photograph of a typical interference pattern is shown in Fig. 3.3.

The relation between the indentation spacing and the fringe order is set by the following equation (Ref 9):

$$d \sin \alpha_0 = m\lambda \quad (3-1)$$

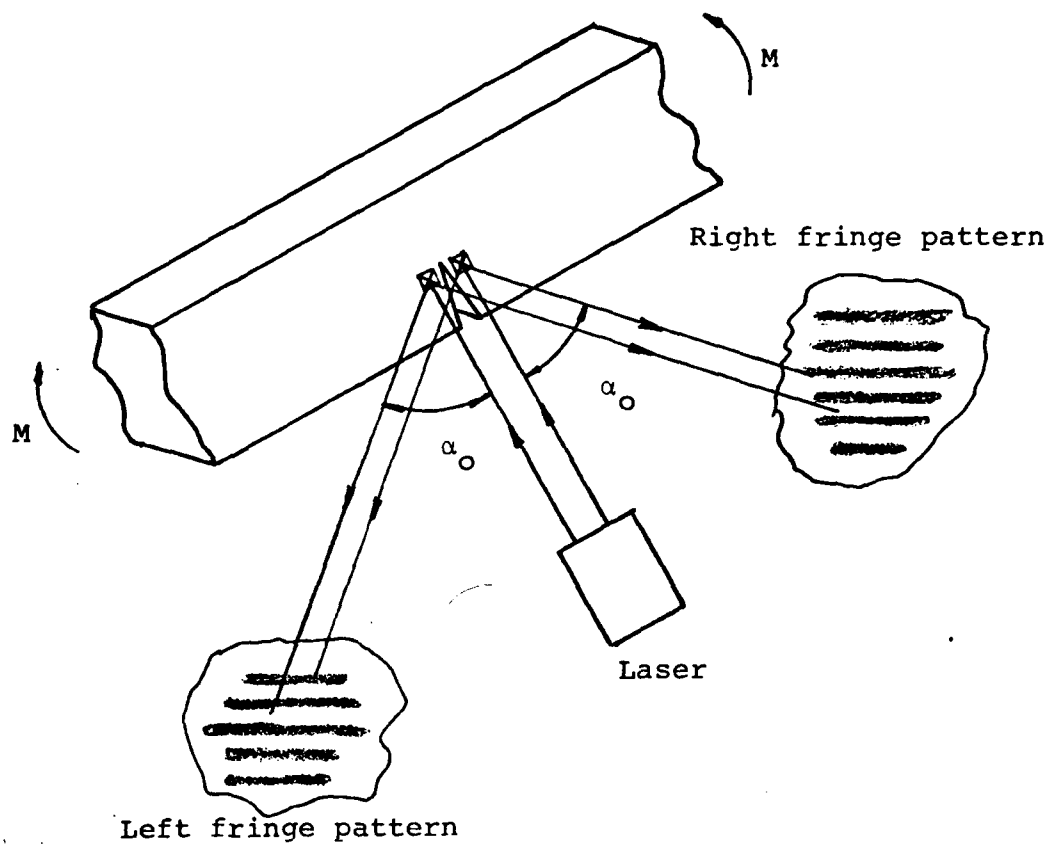


Fig. 3.2. Schematic Showing Fringe Pattern Generation

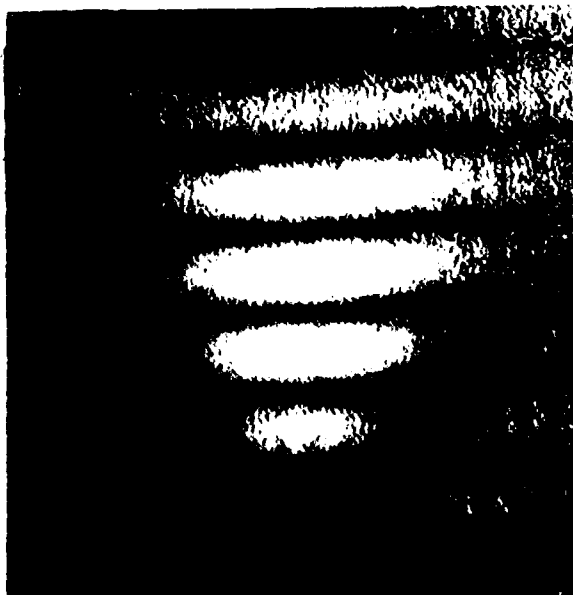


Fig. 3.3. Typical Interference Fringe Pattern

where d is the distance between indentations, λ is the wave length of the source and m is the fringe order.

As a load is applied to the specimen, the crack opens and the distance between the indentation changes. The relation between the change in d and the change in the fringe order δm from a fixed point of view is

$$\delta d = \delta m \lambda / \sin \alpha_0 \quad (3-2)$$

Now observing the fringe pattern from a fixed point allows one to count the number of fringes passing and hence determine the change in the fringe order. Eq (3-2) will then give the change in the distance d between the indentations that correspond to the crack opening. Averaging the left and right fringe number will eliminate free body motion.

Test Apparatus

The test specimens used were flat strips of Aluminum 7075 T651. A small V notch was placed on the edge of the specimen to allow precracking and a shallow groove was cut at the edge as to fit the clip gage used to measure crack mouth openings. (See Fig. 3.4.)

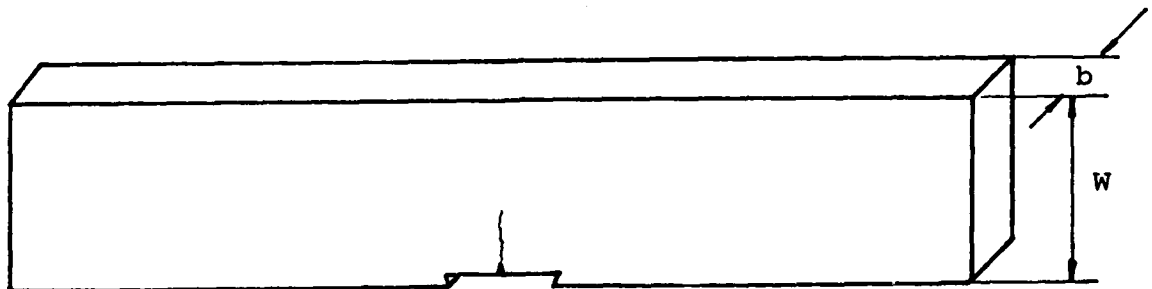


Fig. 3.4. Test Specimen

The specimen was placed in a four-point bending fixture. Load was applied by a standard Instron machine equipped with a compression load cell (Fig. 3.5).

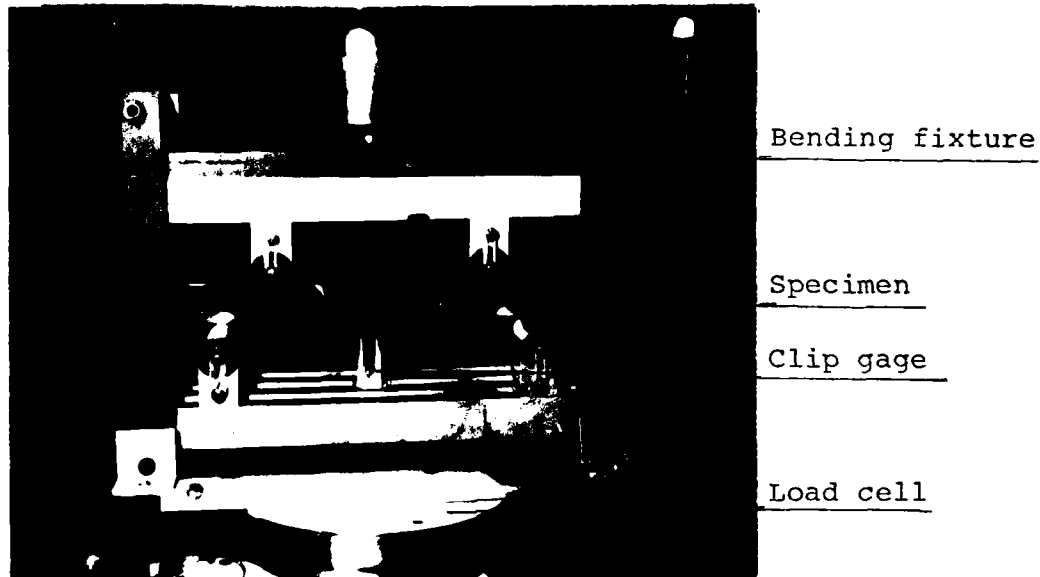


Fig. 3.5. Specimen Set Up in Bending Fixture

The crack mouth opening was measured by a "clip gage" placed in the premachined groove. The "clip gage" consists of two small steel plates on which strain gages were bonded (Fig. 3.6). Precalibrating the "clip gage" allows one to relate the mouth opening with the changes in strain measured.

Two pyramid type indentations have been placed near the crack tip by a standard Lietz microhardener tester with a diamond indenter of a square based pyramid shape with face angles of 136 degrees. The indentations were

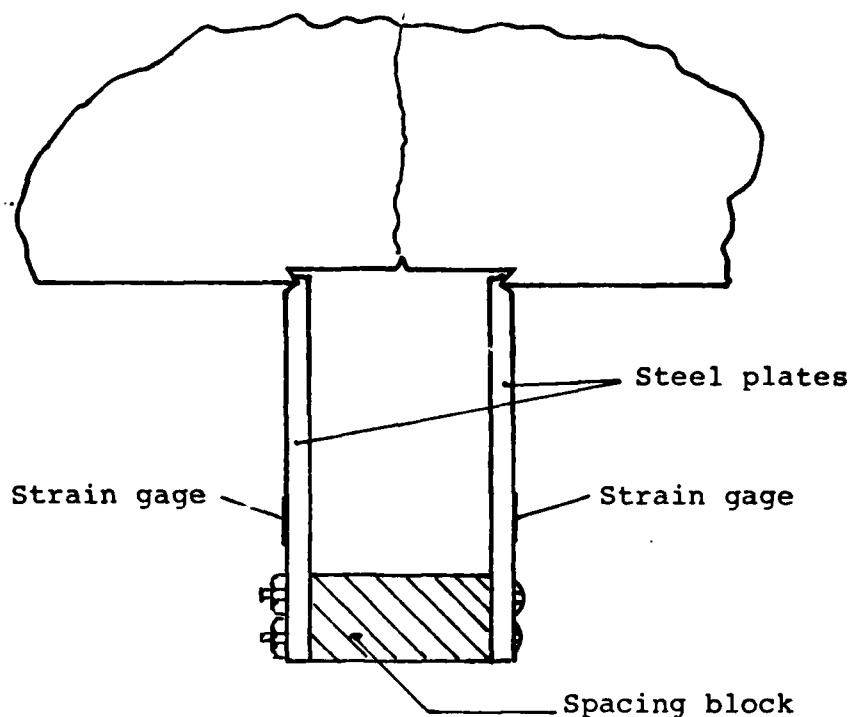


Fig. 3.6. Clip Gage Setup

impinged by a Spectra Physics Model 120 5 MW HeNe laser. The laser beam wave length λ was 0.6328 microns and had a divergence angle of 0.71 mr and a beam diameter of 0.57 mm. The laser was located so that the beam impinged perpendicular to the specimen surface. The angle of the diffracted beam α_0 can be calculated directly by knowing the face angle of the indentation. (See Fig. 3.7.)

The fringes created by the interference of the reflected beams were picked up by two photoresistors that were located in a fixed place on the fringe pattern.

The active face of the photo resistors was masked leaving a narrow slit (smaller than the fringe spacing)

to allow effective distinction between individual fringes. A photograph of the test apparatus is seen in Fig. 3.8.

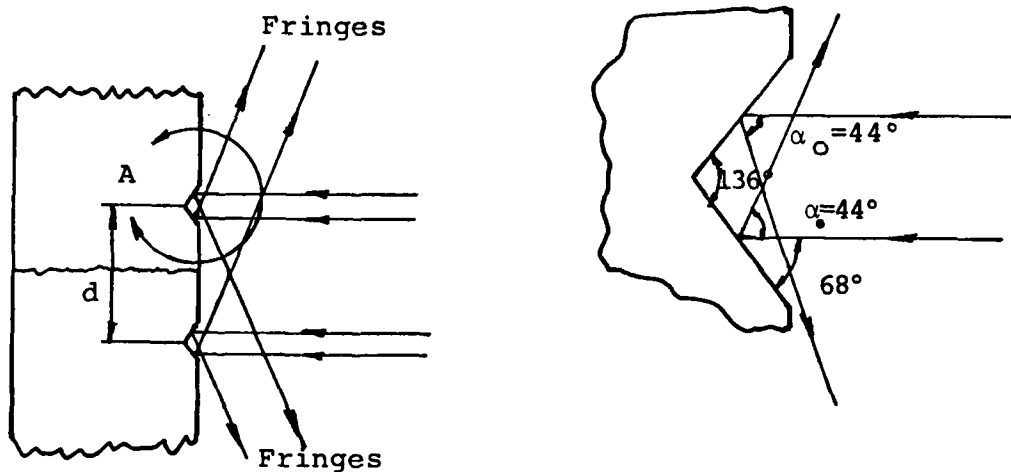


Fig. 3.7. Laser Beam Reflection

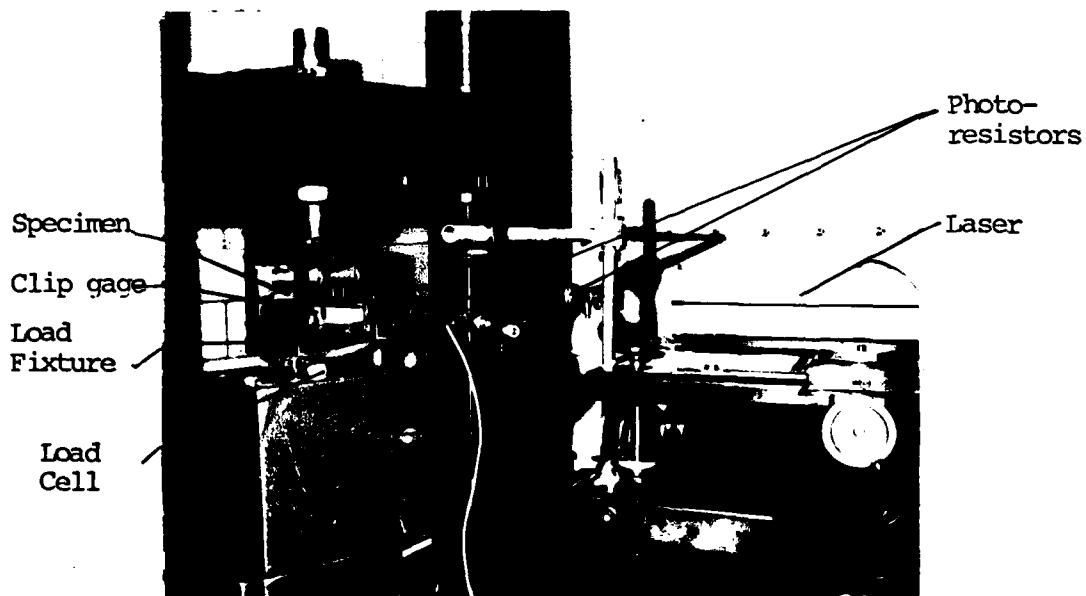


Fig. 3.8. Test Apparatus Setup

As load was applied and the fringes started moving the photoresistor created an electrical signal that after proper amplification could be recorded with the aid of a strip chart recorder.

Test Procedure

Two Aluminum 7075 T651 specimens were each used to test 5-10 different crack lengths. The first specimen was used for longer cracks and the second for shorter cracks with some overlapping between the regions that allowed comparing between the two. The specimens were precracked in the long transverse (LT) direction of the material in three-point bending on a Schenck fatigue machine using cyclic loads at a frequency of 20 Hz. The precracking stress intensity factor varied from 6000-9000 psi $\sqrt{\text{in}}$. The higher K_I was used to initiate and propagate the crack to about 80 percent of the desired length, and the lower K_I levels were applied to get the final sharp crack.

Two indentations were placed on the surface 50-200 microns behind the crack tip as explained previously. A load of 200 grams on the indenter diamond head was found most suitable to create good reflecting indentations with a base square dimension of approximately 30 microns. The specimen was mounted on the loading fixture, the two photoresistor output signals together with the clip gage and load cell signals were monitored by a four-channel strip chart recorder to create a common time basis.

The specimens were loaded typically to values of $K_I = 12-14 \text{ ksi } \sqrt{\text{in}}$ so the amount of plasticity in the specimen was kept small (see Appendix B). Two load cycles were applied prior to actual testing so that the crack would appear to its full length on the surface and would easily be seen under a microscope.

During the preload cycle the photoresistors were relocated to a position such that the maximum fringe intensity could be observed. Since the photoresistors were fixed in position while the specimen with the indentation was displacing due to the applied load, it became necessary to establish the final location of the resistors under a mean load so that the indentations could still stay within the beam boundaries over the extreme deflection.

Three load cycles were applied to each specimen for each crack length. After each test the crack length was measured in order to account for any crack propagation during the test cycle. Then the crack was propagated to the next stage in the Schenck fatigue machine. In addition, for two different crack lengths the crack surface displacement was measured along the crack at 2-6 different locations using previously applied indentations in order to verify the Orange (Ref 11) conic section approximation for the crack opening.

IV. Data Reduction and Numerical Technique

K_I For Case 1

The fringe patterns, crack mouth opening and loads were all recorded on a four-channel strip chart recorder. A typical chart for a single loading cycle is shown in Appendix C, Fig. C.1.

As explained previously, two sets of fringes were created by the reflected beam from the indentation. For each set of fringes, a slope of number of fringes per unit load $\delta m/P$ can be obtained. These slopes were averaged to eliminate free body motion. A more detailed description of the laser interferometer data reduction procedure can be found in Appendix C.

Using Eq (3-2)

$$\frac{n}{P} = \frac{1}{2} \frac{\delta d}{P} = \frac{1}{P} = \frac{1}{2} \frac{\delta m}{P} \cdot \frac{\lambda}{\sin \alpha_0} \quad (4-1)$$

where $\lambda/\sin \alpha_0$ is the calibration factor of the interferometer used here. Eq (4-1) allows one to compute the displacement per unit load. The loading and unloading results of three loading cycles were averaged to give an average displacement per unit load. The distance t of the indentation behind the crack tip was computed by averaging the initial distance before the test with the one measured after three test cycles. Since only three cycles were

applied and the amount of crack propagation was very small (a few microns) linear interpolation was adequate to give a sufficiently accurate estimate.

K_I for Case 1 can now be determined from the crack displacement near the crack tip Eqs (2-12) or (2-14). In most cases θ is close enough to 180° so the simplified form of Eq (2-17) can be used.

Since the measurements are on the surface, the stress field should be considered as plane stress and H should be given the value of E (1×10^7 for aluminum 7075T651). Now Eq (2-17) takes the form

$$\frac{K_I}{P} = \left(\frac{\eta}{P} \right) \frac{E}{4} \left(\frac{2\pi}{t} \right)^{\frac{1}{2}} \quad (4-2)$$

This data will usually be converted to some nondimensional form.

Crack Mouth Opening

The crack mouth opening η_0 was recorded directly from the "clip gage" readings. The crack mouth opening per unit load was then readily obtained from a η_0 versus P plot using only the linear part of the curve and neglecting the initial nonlinear part which is associated with crack closure effects.

Numerical Technique for K_I Case 2 Computation

The rest of the computation, which involved calculating stress intensity factors for different Case 2

loadings were programmed and handled numerically. The $K_{I(1)}$ data was fitted by a suitable interpolation curve. Interpolated values of $K_{I(1)}$ and $\frac{\partial K_{I(1)}}{\partial a}$ were computed for any desired crack length a/w . In a similar way the crack mouth opening data for Case 1 $\eta_{o(1)}$ was fitted by an interpolating curve that allows one to compute values of η_o and $\frac{\partial \eta_o}{\partial a}$ for the desired points. These interpolations are calculated in a different subroutine so any desired interpolation function can be tried without changing the main program. A comparison table for K_I and η_o for interpolated data versus actual data is printed out so one can judge the accuracy of the interpolation process chosen. Fourth order least square polynomials will give reasonable results in many cases.

Using Orange (Ref 11) conic equation discussed in Appendix E for the crack opening profile the derivative of the crack opening along the crack with respect to the crack length can be computed through Eq (2-27).

Since different factors are used to nondimensionalize the K_I and η_o data, care should be taken to bring all the K_I , $\frac{\partial K_I}{\partial a}$, η_o and $\frac{\partial \eta_o}{\partial a}$ to a common basis. Using Eq (2-9), the weight function is computed for each crack length at any point along the crack. The constant H is determined depending on plane stress or plane strain conditions (see Appendix B). The stress distribution along the crack location for a noncracked body $p(t)$ is supplied

by a separate subroutine and can be easily fitted with available data or some known analytical solution. K_I for Case 2 now is computed through integrating Eq (2-30).

The integral is performed numerically using a Romberg integration scheme (Ref 24). Although the weight function and thus the integrand in Eq (2-30) is singular at the crack tip, the integral will still converge to a distinct value quite rapidly for most $p(t)$ functions. Because of the crack tip singularity the lower limit of this integral cannot be set to zero. A value close to zero should be taken and this value can be made smaller and smaller by an iterative process until the value of the integral converges within a specified accuracy.

Since the numerical integration process may be executed many times until convergence is obtained, an efficient algorithm should be used to reduce the required computer time. Romberg integration scheme used here is a powerful and efficient numerical integration technique. It is based upon the trapezoidal rule combined with Richardson extrapolation. More details of this scheme can be found in Hornbeck (Ref 24). Using this scheme reduced the computer time by a factor of about 200 compared to the Simpson's rule integration scheme. A detailed description of the computer program is presented in Appendix D.

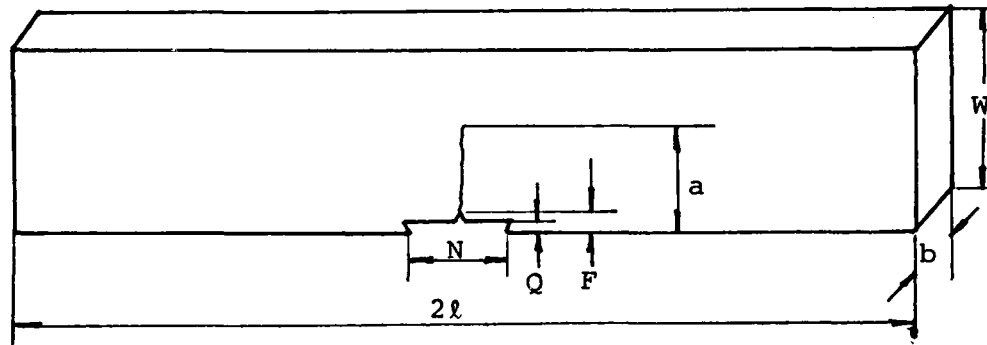
V. Experimental Results

Experimental Measurements

Two Aluminum 7075 T651 edge cracked strips were used in the experiments. The specimens were cut out from a rolled plate and the crack was grown in the long transverse (LT) direction of the material.

The dimensions of the specimens and the region of crack length in which they were tested are shown in Fig.

5.1.



	$2l$	b	w	N^*	Q	F	a
Specimen A	9"	0.24"	1"	.27"	0.04"	0.05"	0.2328" -0.7517"
Specimen B	9"	0.245"	0.7885"	.31"	0.036"	0.036"	0.08153"-0.3753"

*N dimension determined for clip gage purposes.

Fig. 5.1. Specimen Dimensions

Specimen A was tested with ten different crack lengths with crack length to width ratios ranging from .2328-.7517. Specimen B was tested with five different crack lengths where a/w ranged from .1034-.476. Both specimens were loaded in a four-point bending fixture as shown in Fig. 5.2.

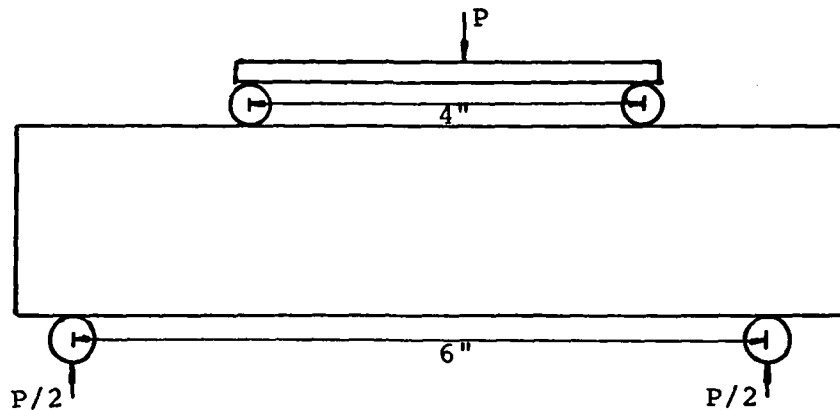


Fig. 5.2. Loading Fixture Dimension

Each specimen was loaded through three loading cycles, and near crack tip displacements (by laser interferometry) and crack mouth openings were recorded. Table I represents the average results for all crack lengths measured.

Data Interpolation

The stress intensity data calculated from the interferometry measurements was converted to a nondimensional form of

$$\frac{K_I}{\sigma\sqrt{\pi a}} = \frac{K_I b W^2}{6M\sqrt{\pi a}} \quad (5-1)$$

TABLE I
Experimental Measurement Results

Specimen	Nondimensional crack length	Distance of indentation from crack tip	No of fringes per unit load	Crack mouth displacement per unit load
	a/w	r	$\delta m/p$	η_o/p
		Microns	$1/lb \times 10^{-3}$	$in/lb \times 10^{-6}$
B	.1034	101	5.093	0.568
B	.1586	83.5	6.623	0.7453
B	.2064	88	7.6713	0.9836
A	.2328	121.5	7.3128	0.856
B	.2646	86.5	9.116	1.268
A	.2666	99.5	7.580	1.14
A	.3094	143	10.180	1.405
A	.346	56	7.340	1.705
A	.3978	72	9.140	2.358
A	.436	46.5	8.0146	2.727
B	.476	47	12.808	4.121
A	.4893	50	10.130	3.6585
A	.5780	111.5	18.354	6.04
A	.6467	74	20.460	9.216
A	.7517	70	35.500	20.681

where M is the bending moment $M = \frac{P \cdot l''}{2}$.

The crack mouth opening data was converted to a nondimensional form

$$\frac{\eta_o}{2\sigma a} \cdot H = \frac{\eta_o b W^2 H}{12 M a} \quad (5-2)$$

The nondimensional data for K_I and η_o was interpolated by a least square fourth order polynomial. Table II and Table III present the actual experimental and the interpolated data for K_I (nondimensional) and η_o (nondimensional) respectively including the relative difference in percent of the interpolating polynomial at the test point.

Fig. 5.3 presents the actual experimental nondimensional K_I compared to the known reference results from Tada (Ref 12). Fig. 5.4 presents the actual experimental nondimensional data for η_o compared to the known reference results from (Ref 12). The average difference between the reference values of K_I and the experimental data is 6% while the maximum difference for a single measurement is up to 14%. These results are similar in accuracy to the ones obtained by Macha (Ref 10) for the laser interferometry technique. The values of K_I from the interpolating polynomial that were actually used to compute the weight function are similar in accuracy with a maximum difference of 13% and an average difference of 6% compared to Ref 12. One should note that the relatively large difference in the slope of $\frac{\partial K_I}{\partial a}$ for some of the short crack lengths

TABLE II

K_I (Nondimensional) Comparison of Actual Data to Interpolated Data

Crack Length	Actual K_I	Interpolated K_I	Relative Difference in %
a/W	$\frac{K_I bW^2}{\sigma M \sqrt{\pi a}}$	$\frac{K_I bW^2}{\sigma M \sqrt{\pi a}} *$	
.1034	.9073	.9467	4.34
.1586	1.0575	.9776	-7.56
.2064	1.0572	1.0545	-.26
.2328	1.1137	1.1060	-.69
.2646	1.1007	1.1705	6.35
.2666	1.1862	1.1746	-.98
.3096	1.2366	1.2590	1.81
.3460	1.3490	1.3244	-1.82
.3978	1.3804	1.4086	2.04
.4360	1.4388	1.4696	2.14
.4760	1.5646	1.5424	-1.42
.4893	1.6551	1.5710	-5.08
.5780	1.8481	1.8774	1.59
.6467	2.3460	2.3688	.97
.7517	3.9513	3.9413	-.25

*The interpolating polynomial is:

$$\frac{K_I bW^2}{\sigma M \sqrt{\pi a}} = 70.75(a/W)^4 - 92.45(a/W)^3 + 42.95(a/W)^2 - 6.53(a/W) + 1.257$$

TABLE III

η_o (Nondimensional) Comparison of Actual Data to Interpolated Data

Crack Length	Actual η_o	Interpolated η_o	Relative Difference in %
a/W	$\frac{\eta_o bW^2H}{12Ma}$	$\frac{\eta_o bW^2H}{12Ma}^*$	
.1034	1.9440	1.9500	.31
.1586	1.6643	1.6491	-.91
.2064	1.6855	1.6334	-3.09
.2328	1.6163	1.6879	4.43
.2646	1.6950	1.7933	5.80
.2666	1.8796	1.8011	-4.18
.3096	1.9961	1.9923	-.19
.3460	2.1660	2.1823	.75
.3978	2.6055	2.4945	-4.26
.4360	2.7493	2.7696	.74
.4760	3.0632	3.1251	2.02
.4893	3.2866	3.2648	-.66
.5780	4.5933	4.6431	1.08
.6467	6.6244	6.5725	-.78
.7517	12.0980	12.1082	.08

*The interpolating polynomial is:

$$\frac{\eta_o bWH}{12Ma} = 210.38(a/W)^4 - 282.57(a/W)^3 + 150.74(a/W)^2 - 32.16(a/W) + 3.952$$

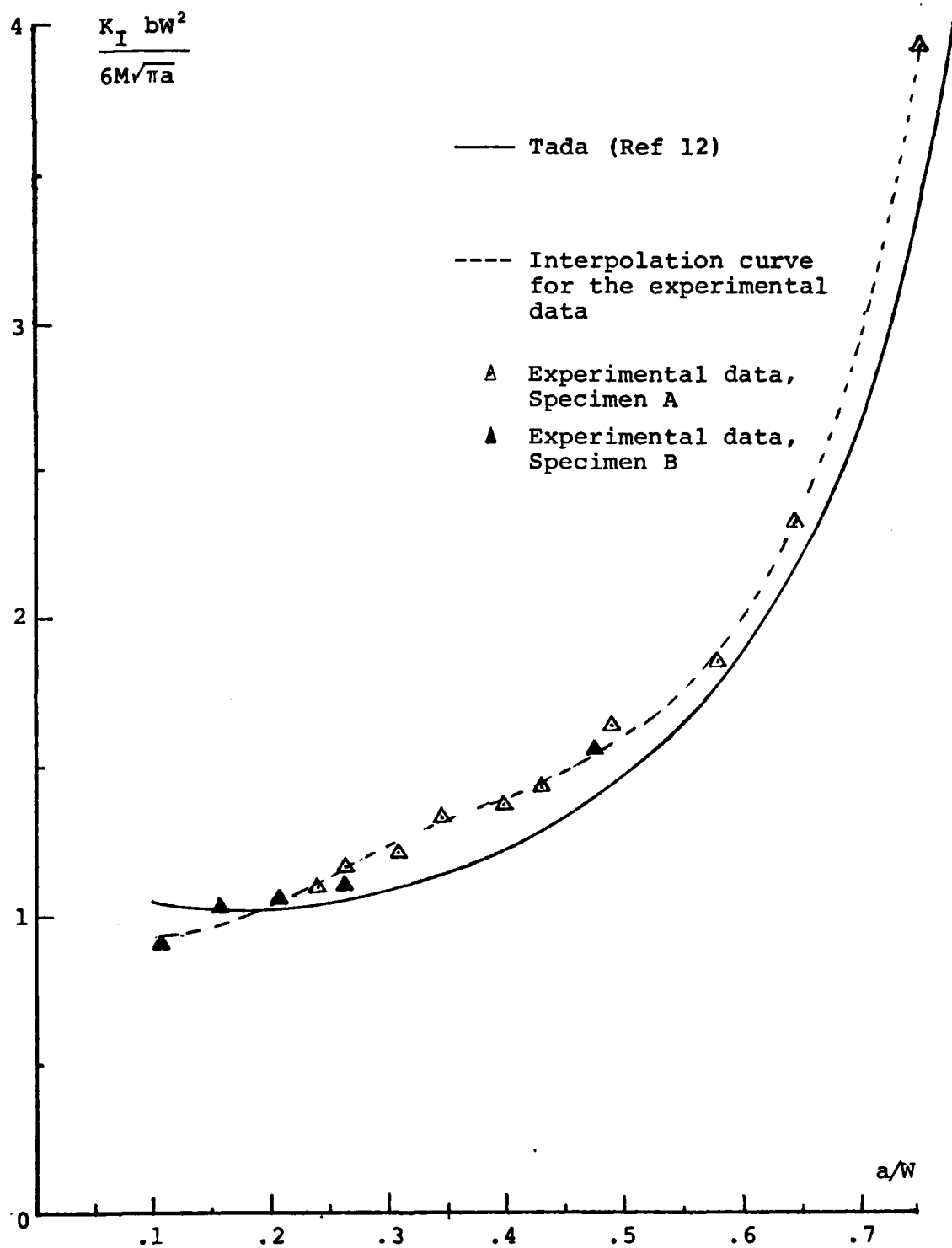


Fig. 5.3. Stress Intensity Factor (Nondimensional)
for Pure Bending

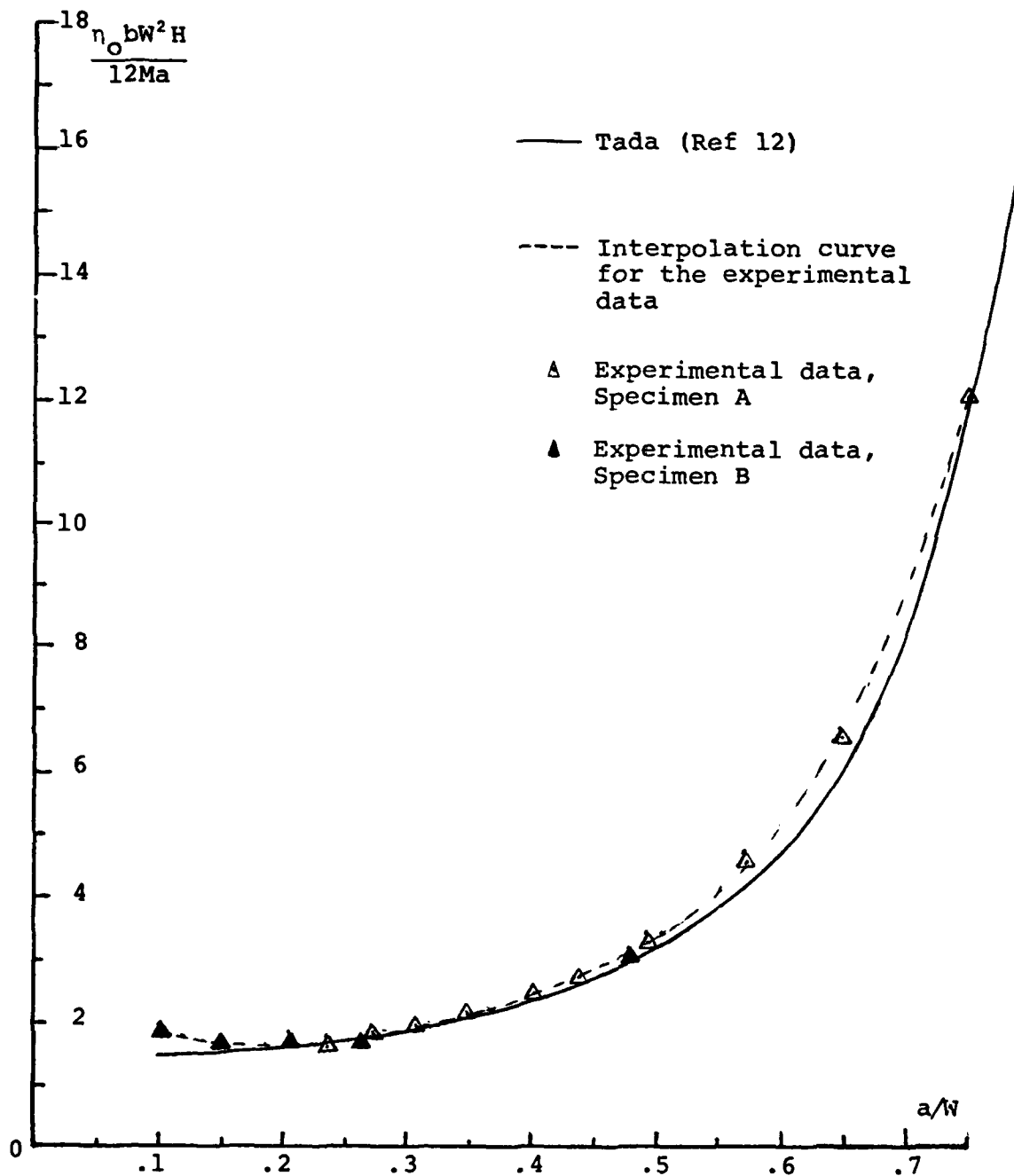


Fig. 5.4. Crack Mouth Opening (Nondimensional)
for Pure Bending

(see Fig. 5.3) will have only a minor influence on the weight function computation as can be seen from examining Eq (2-30). η_0 data as well as the interpolating polynomial fits the reference (12) values much better as seen in Fig. 5.4.

Crack Profile Measurements

For two different crack lengths on specimen A the crack opening was measured along the crack at several points in addition to the point near the crack tip and at the crack mouth. These measurements were done by the laser interferometry technique. The existing indentations left behind as the crack propagated were used for these measurements. The crack openings along the crack were compared to the Orange (Ref 11) conic sections and found to match this approximation excellently (see Figures 5.5 and 5.6).

Case 2 Loadings

Three different loading configurations were chosen for Case 2, uniform tension, three-point bending with S/W of 4 and 8 (see Fig. 5.7). Each of the different Case 2 loading configurations requires another function $p(t)$ as the noncracked body stress at the crack location stresses.

Uniform Tension

In this case,

$$p(t) = \text{const.} = \sigma_0$$

where σ_0 is the remote stress. Since the standard

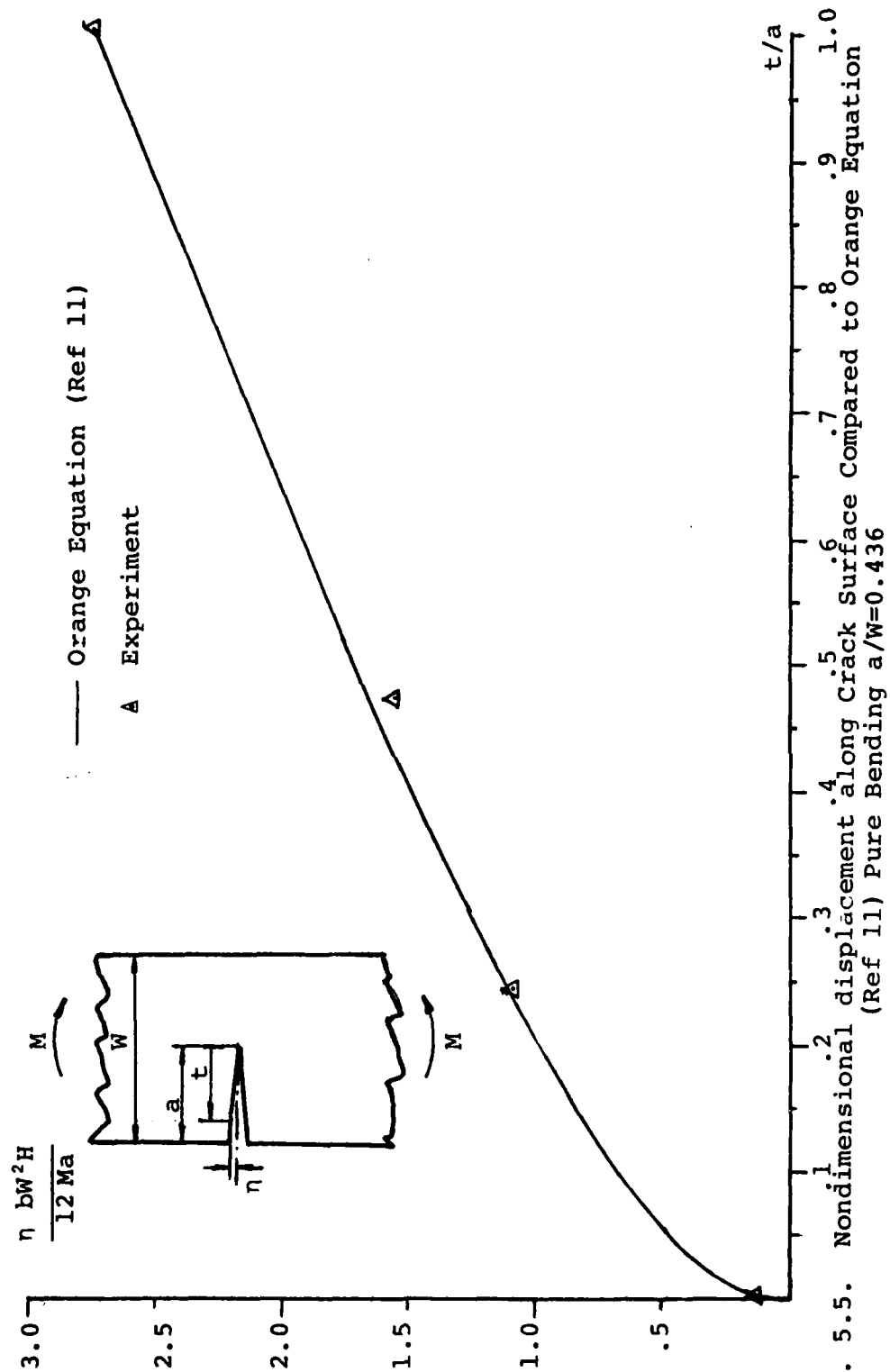


Fig. 5.5. Nondimensional displacement along Crack Surface Compared to Orange Equation (Ref 11) Pure Bending $a/W=0.436$

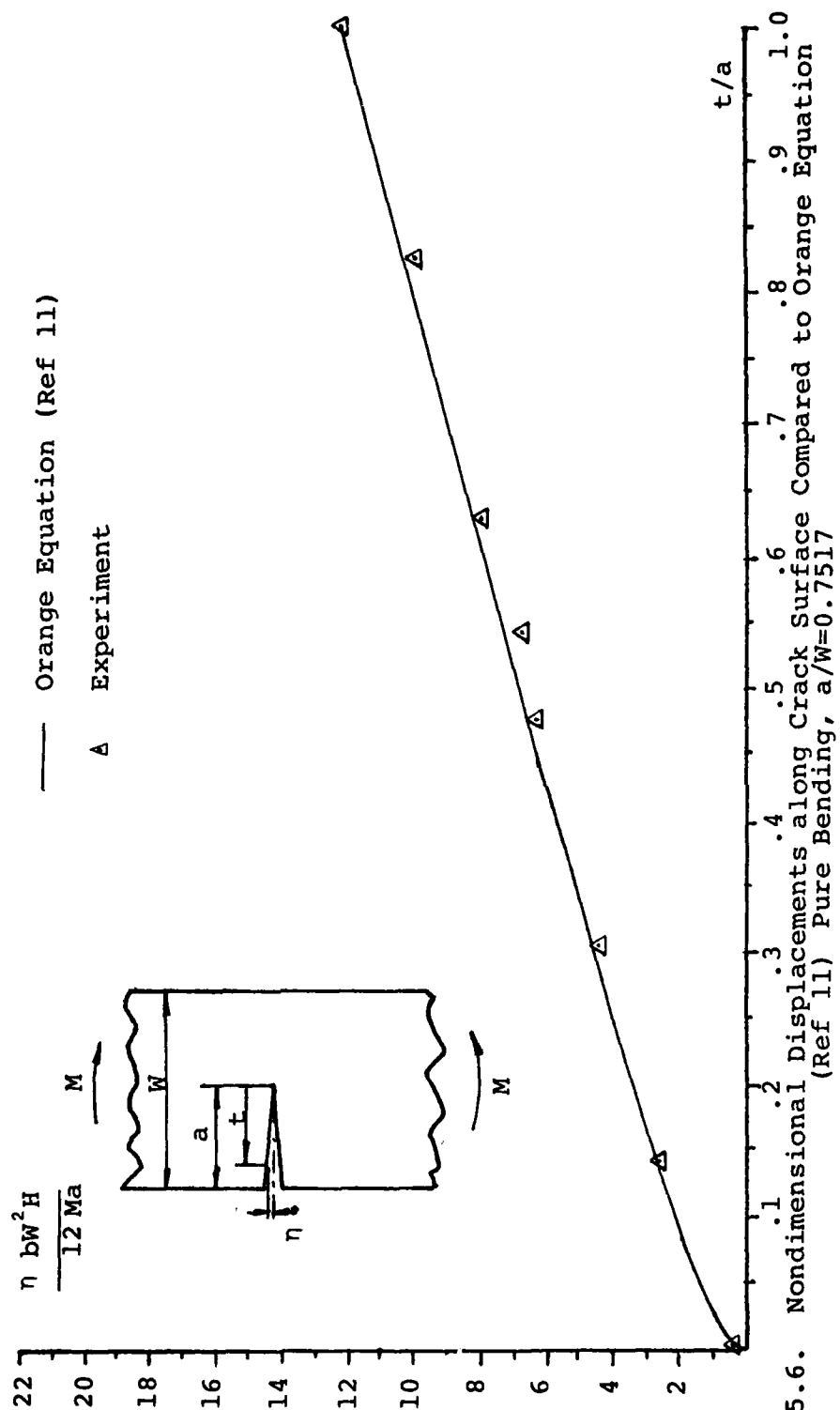


Fig. 5.6. Nondimensional Displacements along Crack Surface Compared to Orange Equation (Ref 11) Pure Bending, $a/W=0.7517$

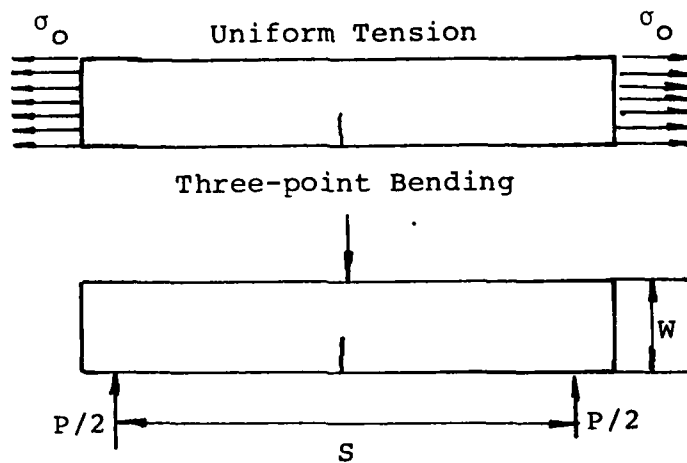


Fig. 5.7. Case 2 Loading Configurations

nondimensional representation for K_I for uniform tension is

$$\frac{K}{\sqrt{\pi a} \sigma_0} \quad (5-4)$$

the function $p(t)$ should be factored by $1/\sqrt{\pi a} \sigma_0$ to get K_I in the desired form. Therefore, take

$$p(t) = \frac{1}{\sqrt{\pi a}} \quad (5-5)$$

(in the computer program $1/\sqrt{\pi a}$ is already factored in the weight function so $p(t)$ is substituted as 1.).

The results of the nondimensional stress intensity factor for uniform tension at equally spaced points from $a/W=.1$ to $a/W=.7$ are presented in Table IV. These results are compared to Tada's (Ref 12) solution. The results agree with the reference solution within 8 percent.

TABLE IV

 K_I (Nondimensional) for Uniform Tension

Crack Length a/W	$\frac{K_I}{\sigma\sqrt{\pi a}}$ Calculated Using the Weight Function	$\frac{K_I}{\sigma\sqrt{\pi a}}$ From Ref 12	Relative Difference in %
.1000	1.2705	1.1957	6.26
.1500	1.2697	1.2682	.12
.2000	1.4041	1.3667	2.74
.2500	1.5540	1.4941	4.01
.3000	1.6855	1.6551	1.83
.3500	1.8170	1.8565	-2.13
.4000	1.9967	2.1080	-5.28
.4500	2.2917	2.4241	-5.46
.5000	2.7719	2.8266	-1.93
.5500	3.4752	3.3486	3.78
.6000	4.3636	4.0432	7.92
.6500	5.3158	4.9993	6.33
.7000	5.1832	6.3755	-3.02

Fig. 5.8 compares the reference solution (Ref 12) to the values calculated at the same a/W points where experiments were performed on the four-point bending specimen. One can see that the last point is the only calculated value that does not agree favorably with the reference data. Since the computations required differentiation of experimental data, one should be very suspicious about the results obtained at the experimental interval end points. Close to the end points computing derivatives actually requires extrapolations that can be very inaccurate, since the behavior of the function is unknown in these regions.

Investigating Eq (2-30) shows clearly that the derivatives $\partial K/\partial a$ and $\partial \eta_0/\partial a$ have a relatively larger influence on the value of the weight function at longer crack lengths; therefore, the computed values are more likely to get distorted at the upper limit of the experimental a/W interval as can indeed be seen in Fig. 5.8.

Three-Point Bending

A solution for the stress distribution of a non-cracked strip under three-point bending in a cross-section through the center is given by Timoshenko (Ref 27):

$$\sigma_x = \frac{3P}{2c^3b} \left(\frac{l}{2} - \frac{c}{\pi} \right) y + \frac{P}{2\pi cb} + \frac{P}{\pi cb} \left(\frac{y^3}{2c^3} - \frac{3}{10} \frac{y}{c} \right) \quad (5-6)$$

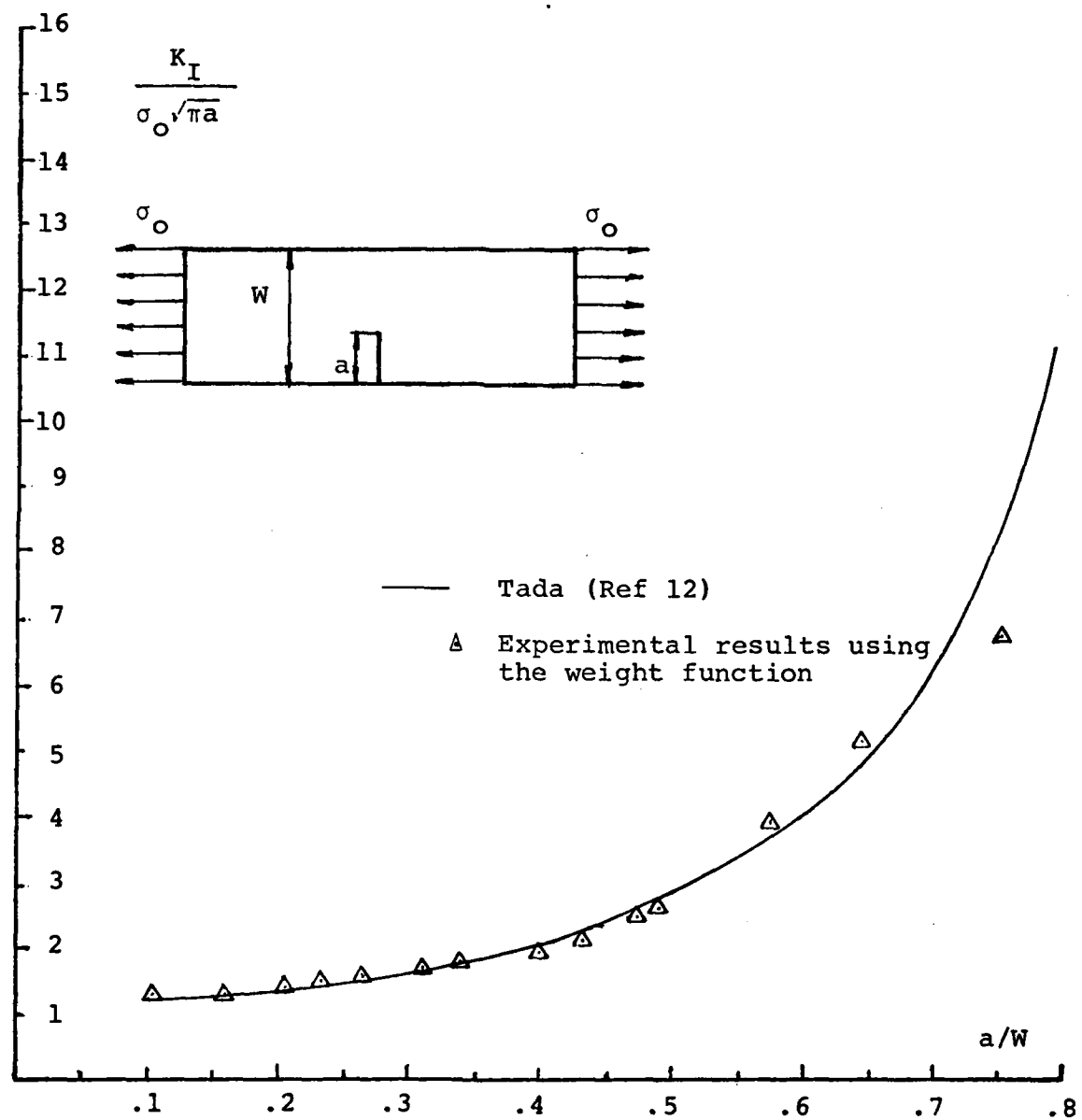


Fig. 5.8. Stress Intensity Factor (Nondimensional)
for Uniform Tension

The terms of this equation are defined in the following Figure 5.9. σ_x is the stress in x-direction along AD.

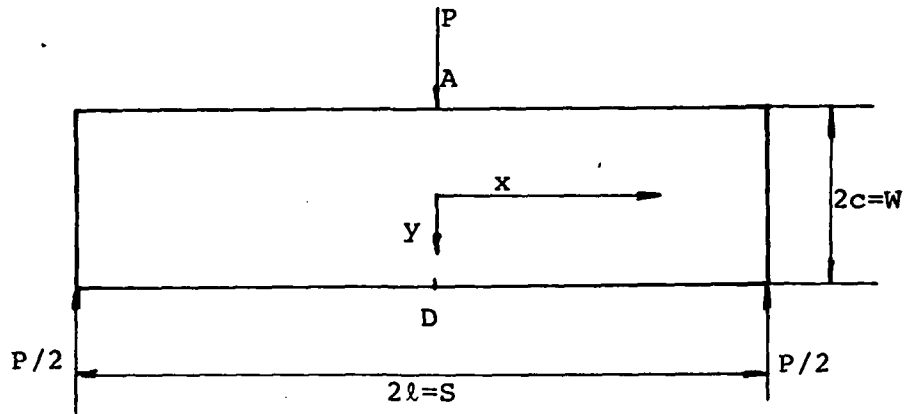


Fig. 5.9. A Uniform Strip Under Three Point Bending

According to Timoshenko, this expression gives the stress with very good accuracy except for point D where an error of $.121 \frac{P}{cb}$ exists based on a more accurate solution. This term will lead in our worst case to an error of 4 percent in the load distribution at the crack mouth location, but since, at this point the weight function has its lowest value, the integral of the product of h and $p(t)$ is expected to have much better accuracy. The standard nondimensional solution is of the form

$$\frac{K_I}{\sigma \sqrt{\pi a}} \quad (5-6a)$$

where $\sigma = \frac{6M}{4bc^2}$ and $M = \frac{Pl}{2}$

So the undimensional form of K_I becomes

$$\frac{K_I}{\sqrt{\pi a}} \frac{4c^2 b}{3Pl} \quad (5-7)$$

The factor $1/\sqrt{\pi a}$ is already included in our computer program in the weight function so the form of $p(t)$ that is required in order to get K_I in the form of Eq (5-7) is

$$p(t) = \frac{\sigma_x(t) 4bc^2}{3Pl} \quad (5-8)$$

Substituting Eq (5-6) to Eq (5-8) yields

$$p(y) = \frac{2}{3\pi} \left(\frac{c}{\ell} \right) + \left[1 - \frac{12}{5\pi} \left(\frac{c}{\ell} \right) \right] \frac{y}{c} + \frac{2}{3\pi} \left(\frac{c}{\ell} \right) \left(\frac{y}{c} \right)^3 \quad (5-9)$$

where $S = 2\ell$

and $W = 2c$

Changing to crack tip coordinates t the expression for y/c becomes

$$y/c = \frac{1}{(W/2)} \left(t + \frac{W}{2} - a \right) = 2 \left(\frac{t}{W} - \frac{a}{W} \right) + 1 \quad (5-10)$$

Substitute Eq (5-10) into Eq (5-9) and get

$$p(t) = \frac{2}{3\pi} \left(\frac{S}{W} \right) + \left[1 - \frac{12}{5\pi} \left(\frac{S}{W} \right) \right] \left[2 \left(\frac{t}{W} - \frac{a}{W} \right) + 1 \right] + \frac{2}{3\pi} \left(\frac{S}{W} \right) \left[2 \left(\frac{t}{W} - \frac{a}{W} \right) + 1 \right]^3 \quad (5-11)$$

Results for the nondimensional stress intensity factor considering three-point bending ($S/W=4$ and $S/W=8$) are presented in Tables V and VI respectively. These results are compared with known results from Ref 12 and Ref 28. The reference solution claims to be accurate for $a/W < 6$ and in this interval the calculated experimental values are within 6.15 percent accuracy for $S/W=4$ and 5.9 percent for $S/W=8$.

Fig. 5.10 and Fig. 5.11 show the calculated K_I for three-point bending for the a/W points where actual data was gathered for the four-point bending. As for the uniform tension case the last point is the only one not fitting the expected curve because of the inaccurate extrapolation procedure explained previously.

TABLE V

 K_I (Nondimensional) for Three-Point Bending, $S/W=4$

Crack Length a/W	K_I (Nondimensional) Calculated Using the Weight Function	K_I (Nondimensional) Ref 28	Relative Difference in %
.1000	1.0134	.9849	2.89
.1500	.9447	.9731	-2.91
.2000	.9838	.9803	.36
.2500	1.0272	1.0037	2.34
.3000	1.0491	1.0425	.64
.3500	1.0635	1.0979	-3.13
.4000	1.1015	1.1736	-6.15
.4500	1.1994	1.2754	-5.96
.5000	1.3866	1.4112	-1.74
.5500	1.6656	1.5910	4.69

TABLE VI

 K_I (Nondimensional) for Three-Point Bending, $S/W=8$

Crack Length a/W	K_I (Nondimensional) Calculated Using the Weight Function	K_I (Nondimensional) Ref 28	Relative Difference in %
.1000	1.0630	1.0156	4.66
.1500	.9911	1.0080	-1.68
.2000	1.0314	1.0183	1.28
.2500	1.0755	1.0438	3.04
.3000	1.0964	1.0839	1.15
.3500	1.1087	1.1403	-2.77
.4000	1.1450	1.2167	-5.89
.4500	1.2431	1.3189	-5.75
.5000	1.4328	1.4549	-1.52
.5500	1.7160	1.6349	4.96

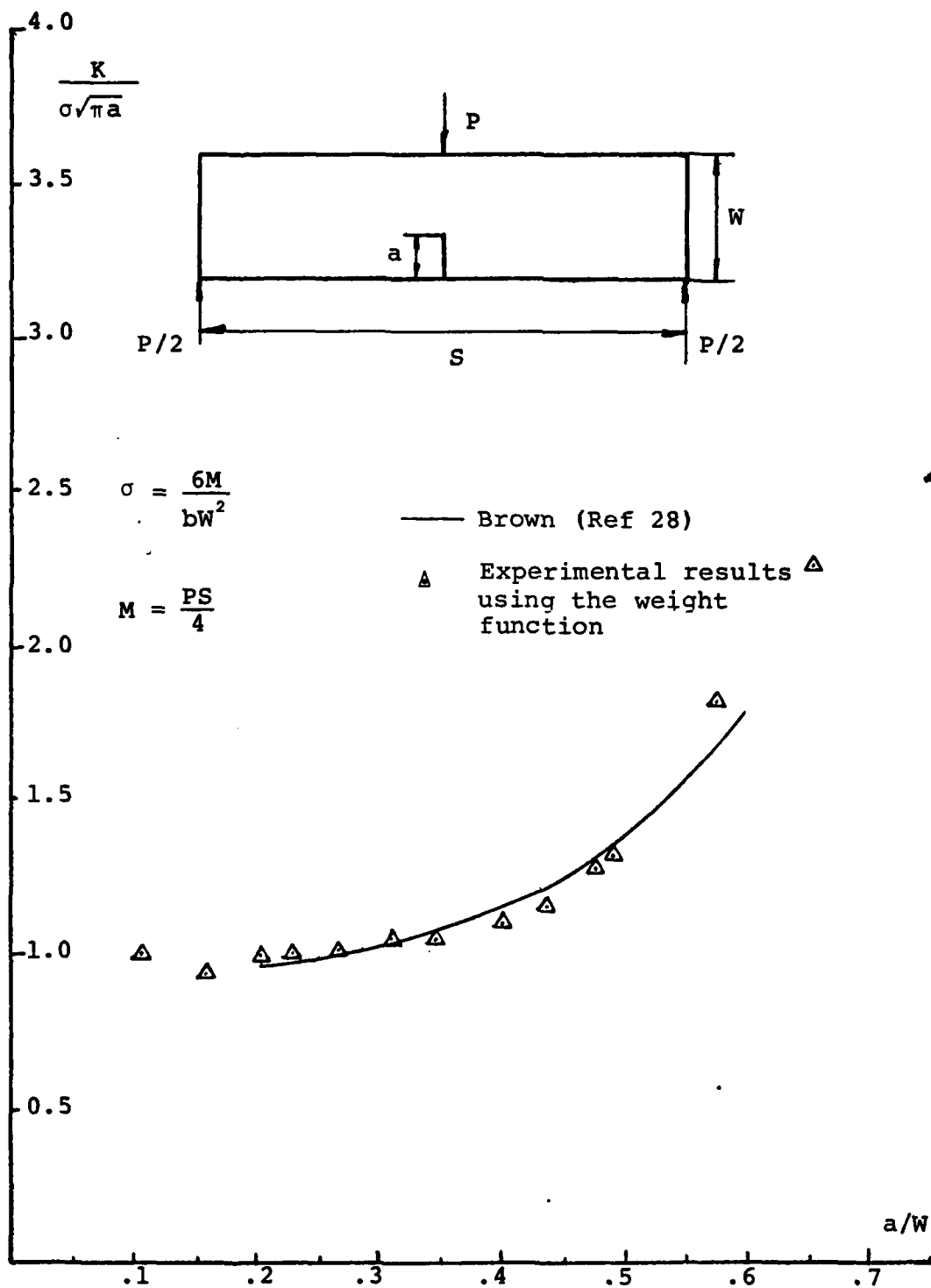


Fig. 5.10. Stress Intensity Factor (Nondimensional) for Three-Point Bending $S/W=4$

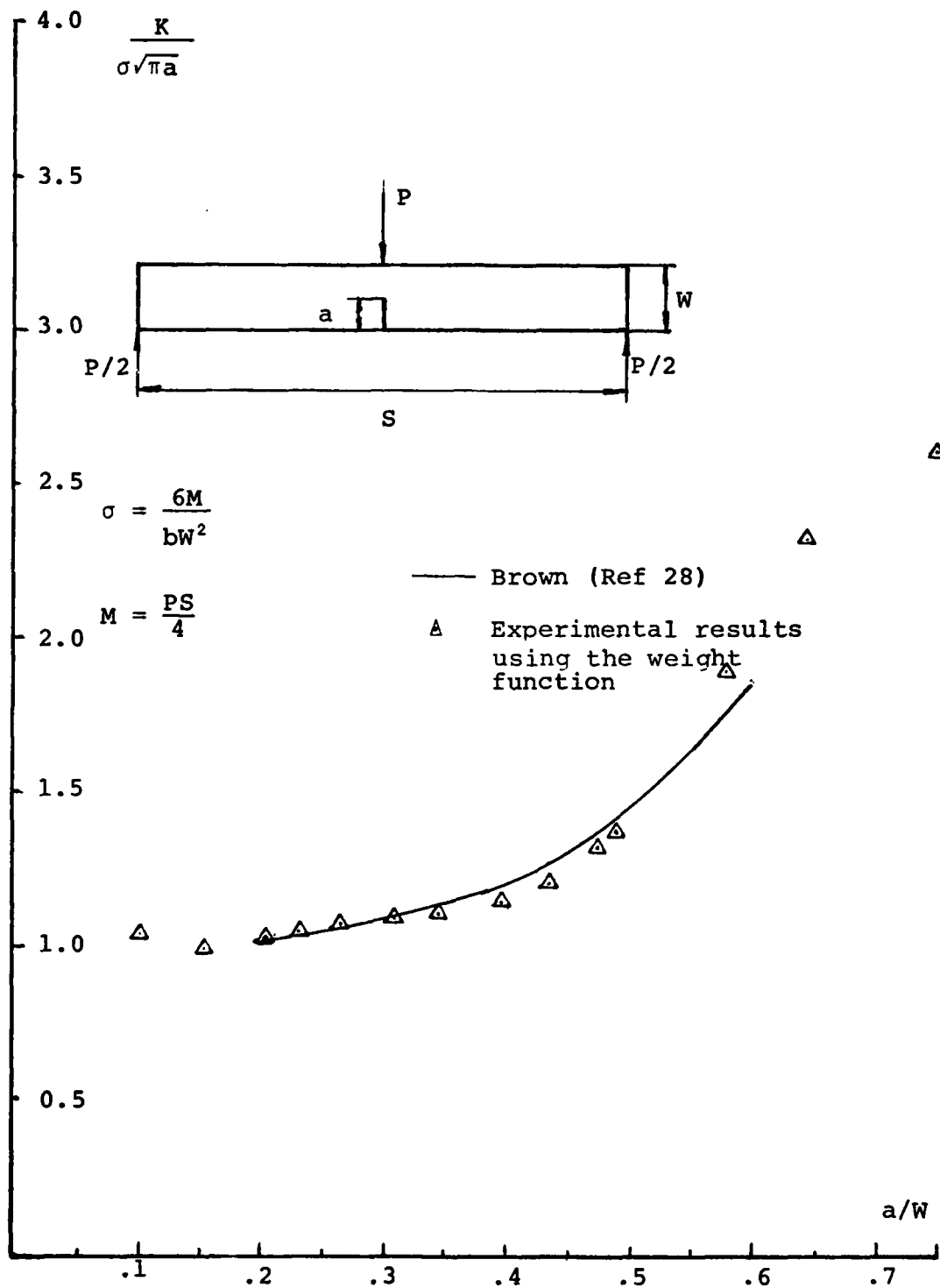


Fig. 5.11. Stress Intensity Factor (Nondimensional) for Three-Point Bending, $S/W=8$

VI. Conclusions

1. This work shows clearly that the experimental weight function procedure leads to excellent results for the stress intensity factor without actually testing the loading configuration in question.

2. A set of experiments of a single loading configuration can be used to calculate the stress intensity factor solution for any other loading configuration applied to the same geometry. The only additional information required is the stress distribution at the crack location for a noncracked body.

3. One should limit the results obtained for a different loading only to the same a/W region studied in the original experiment. Extrapolations, or even calculations, near the test a/W limits may lead to inaccurate results.

4. Because data scatter can lead to errors when differentiated, care should be taken to collect enough data to yield reasonable interpolating functions.

5. Even though some error was introduced in the K_I and η_O measurements, the numerical procedure using the derivatives of K_I and η_O did not distort the Case 2 results beyond the basic accuracy of the Case I measurements.

6. The laser interferometric technique provides an efficient procedure for crack opening measurements and leads to accurate results for this type of measurement.

7. The Orange (Ref 11) conic section again provided an accurate representation for the crack opening profile for edge cracked strips. This conic section should, however, be compared with actual profile measurements (as done here) prior to applying it to other geometries.

8. The fact that the actual cracks were not perfectly straight on a micro-scale, as assumed in this theory, is the most likely source for K_I calibration errors for Case 1 loading (four-point bending). Perhaps other materials would give "straighter" cracks which more closely match the analytical behavior.

Bibliography

1. Griffith, A. A. "Transactions Royal Society of London," Vol. 221, 1920 (this article has been published in Trans., ASM, 61, 1968, p. 871).
2. Bueckner, H. F. A Novel Principle for the Computation of Stress Intensity Factors. ZAMM, 50, 1970, pp. 529-546.
3. Rice, J. R. Some Remarks on Elastic Crack Tip Stress Fields. Technical Report, NASA NGL 40-002-08015, June 1971.
4. Bueckner, H. F. "Weight Functions for the Notched Bar," Zeitscheift für Angewandte Mathematik und Mechanik, Vol. 51, 1971, pp. 97-109.
5. Paris, P. C., McMeeking, R. M., and Tada, H. The Weight Function Method for Determining Stress Intensity Factors. MRL E-92. Material Research Laboratories, Brown University, 1975.
6. Grandt, A. F., Jr. "Stress Intensity Factors for Some Through-Cracked Fastner Holes," International Journal of Fractures, Vol. 11, No. 2, April 1975.
7. Petroski, H. J., and Achenbuch, J. D. "Computation of the Weight Function from a Stress Intensity Factor," Engineering Fracture Mechanics, Vol. 10, No. 2, pp. 257-266.
8. Labbens, R., and Heliot, Jr. 8th National Symposium of Fracture Mechanics. August 26-28, Brown University.
9. Sharpe, W. N., Jr., and Grandt, A. F., Jr. A Laser Interferometric Technique for Crack Surface Displacement Measurement. Air Force Material Laboratories, AFML-TR-74-75, July 1974.
10. Macha, D. E., Sharpe, W. N., Jr., and Grandt, A. F., Jr. A Laser Interferometry Method for Experimental Stress Intensity Factor Calibration, Cracks and Fracture. ASTM STP 601, American Society for Testing and Materials, 1976, pp. 490-505.

11. Orange, T. W. Crack Shapes and Stress Intensity Factors for Edge-Cracked Specimens Stress Analysis and Growth of Cracks. Proceedings of the 1971 National Symposium on Fracture Mechanics, Part I, ASTM STP 513, American Society for Testing and Materials, 1972, pp. 71-78.
12. Tada, H., Paris, P. C., and Irwin, G. R. The Stress Analysis of Cracks Handbook. DEL Research Corporation.
13. Rooke, D. P., and Cartwright, D. J. Stress Intensity Factors.
14. Grandt, A. F., Jr. Lecture Notes MC 6.05 Linear Elastic Fracture Mechanic. School of Engineering, Air Force Institute of Technology, Wright-Patterson AFB, 1978.
15. Hertzberg, R. W. Deformation and Fracture Mechanics of Engineering Materials. New York: John Wiley & Sons, Inc., 1976.
16. Damage Tolerant Design Handbook. MCIC-HB-01. Metals & Ceramics Information Center, Battelle-Columbus Laboratories, 1972.
17. Eftis, J., Subramonian, N., and Liebowitz, H. "Crack Border Stress and Displacement Equations Revisited, Engineering Fracture Mechanics, Vol. 9, 1977, pp. 189-210.
18. Packman, P. F. The Role of Interferometry in Fracture Studies. Vanderbilt University, Nashville, TN.
19. Sharpe, W. N., Jr., and Grandt, A. F., Jr. A Preliminary Study of Fatigue Crack Retardation Using Laser Interferometry to Measure Crack Surface Displacement, Mechanics of Crack Growth. ASTM STP 590. American Society for Testing and Materials, 1976, pp. 302-320.
20. Gross, B., Roberts, E., Jr., and Srawley, J. E. "Elastic Displacements for Various Edge-Cracked Plate Specimens," The International Journal of Fracture Mechanics, Vol. 4, No. 3, September 1968.
21. Grandt, A. F., Jr. Two Dimensional Stress Intensity Factor Solutions for Radically Cracked Rings. AFML-TR-75-121, Air Force Material Laboratories, Wright-Patterson Air Force Base.

22. Irwin, G. R. Fracturing of Metals. ASM, Cleveland, Ohio, 1949, p. 147.
23. Gallagher, J.P. What the Designer Should Know About Fracture Mechanics Fundamentals. Automotive Engineering Congress, Detroit, Michigan, January 1971.
24. Hornbeck, R. W. Numerical Methods, QPL Series. New York: Quantum Publishers, Inc.
25. Subprogram Library Guide. ASD Computer Center, Wright-Patterson Air Force Base, Ohio.
26. IMSL Library Guide. IMSL, International Mathematical and Statistical Library, Houston, Texas.
27. Timoshenko, S. P., and Goodier, J. N. Theory of Elasticity. New York: McGraw-Hill, 1969.
28. Brown, W. F., Jr., and Srawley, J. E. Plane Strain Crack Toughness Testing of High Strength Metallic Materials. ASTM STP 410, American Society for Testing and Materials, 1967, p. 13.

Appendix A
The Weight Function

The idea of the weight function has been introduced by Bueckner (Ref 2) and was also discussed in (Refs 2-8).

The following analysis shows that if the complete solution of the stress intensity factor and the crack opening displacement for a crack subjected to a certain loading system is known, then the stress intensity factor solution for the geometry under another loading configuration may be obtained directly from the known solution.

Let us consider a cracked body with loads P_1, \dots, P_n as described in Fig. A.1.

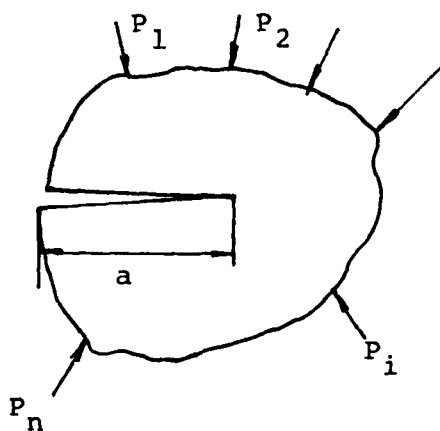


Fig. A.1. Loaded Cracked Body

The elastic energy release rate, often referred to as the Griffith energy rate, can be defined following Irwin (Ref 22) as

$$\mathcal{G} = \left. \frac{\partial U}{\partial a} \right|_P \quad (A-1)$$

where U is the total potential energy stored in the cracked body and a is the crack length.

\mathcal{G} has units of force and is often referred to as the crack extension force

$$U = \frac{1}{2} \sum_{i=1}^N \sum_{j=1}^N C_{ij} P_i P_j \quad (A-2)$$

where C_{ij} is the compliance coefficient defined as the deflection at point i due to a unit force at point j .

$$\mathcal{G} = \left. \frac{\partial U}{\partial a} \right|_P = \frac{1}{2} \sum_{i=1}^N \sum_{j=1}^N \frac{\partial C_{ij}}{\partial a} P_i P_j = \frac{1}{2} \sum_{i=1}^N \frac{\partial u_i}{\partial a} \cdot P_i \quad (A-3)$$

where

$$u_i = \sum_{j=1}^N u_i^j = \sum_{j=1}^N C_{ij} P_j \quad (A-4)$$

u_i^j is the displacement at i due to load P_j .

Since the elastic energy release rate \mathcal{G} (based on strain energy consideration) and the stress intensity factor K (based on crack tip stress considerations) are both parameters that characterize crack growth, a relation can

be established between them as shown by Hertzberg (Ref 15).

$$\mathcal{G} = \frac{K^2}{H} \quad (A-5)$$

where H is defined as

$$H = \begin{cases} E & \text{for plane stress} \\ \frac{E}{1-\nu^2} & \text{for plane strain} \end{cases} \quad (A-6)$$

Since K is the linear elastic stress intensity factor, superposition can be used to write

$$K = \sum_{i=1}^N K_i = \sum_{i=1}^N k_i(a) P_i \quad (A-7)$$

k_i stress intensity factor per unit load. Substituting, into the elastic energy release rate

$$\mathcal{G} = \frac{K^2}{H} = \frac{1}{H} \sum_{i=1}^N \sum_{j=1}^N k_i(a) k_j(a) P_i P_j \quad (A-8)$$

By equating the Eq (A-8) to Eq (A-3) we conclude that they should be equal term by term.

Thus,

$$\frac{k_i(a) k_j(a)}{H} = \frac{1}{2} \frac{\partial C_{ij}(a)}{\partial a} \quad (A-9)$$

If the full solution for K is known only for one load, say P_m , then

$$k_i(a) = \frac{H}{2} \frac{\partial C_{im}(a)}{\partial a} \cdot \frac{1}{k_m(a)} \quad (A-10)$$

recall, that we defined in Eq (A-7) $k_m = \frac{K_m}{P_m}$

and in Eq (A-4) $C_{im} = \frac{u_i^m}{P_m}$

Therefore,

$$k_i(a) = \frac{H}{2} \frac{\partial u_i^m}{\partial a} \frac{1}{K_m} \quad (A-11)$$

and since

$$K = \sum_{i=1}^N k_i(a) P_i \quad (A-12)$$

Then

$$K = \frac{H}{2K_m} \sum_{i=1}^N \frac{\partial u_i^m}{\partial a} P_i \quad (A-13)$$

For an arbitrary distribution of P_i , and a set of surface tractions $T(s)$, the expression for K can be written as

$$K = \frac{H}{2K_m} \int_s \frac{\partial u^m}{\partial a}(s,m) T(s) ds \quad (A-14)$$

If one defines the weight function as

$$h_m(s,a) = \frac{H}{2K_m(a)} \frac{\partial u^m(s,a)}{\partial a} \quad (A-15)$$

Then we can readily see that the weight function depends only on the geometry of the cracked body (including the

crack length) and the loading configuration denoted by the superscript m.

Substituting the term for the weight function into Eq (A-14), we get

$$K = \int_s h_m(s,a) T(s) ds \quad (A-16)$$

We can therefore conclude that the stress intensity factor for the arbitrary surface traction $T(s)$ can be obtained from the known weight function we computed considering the loading configuration m. In a little bit more general derivation, the body forces can be included and one can write

$$K = \int_{\Gamma} T \cdot h d\Gamma + \int_A f \cdot h \cdot dA \quad (A-17)$$

where h is the weight function obtained from any known load configuration,

T are the surface traction for which K is to be determined,

f are the body forces for which K is to be determined,

Γ is a chosen path around our specimen as to include all the surface tractions T , and

A is the region where the body forces act.

Appendix B
Justification of Assumptions

Use of Linear Elastic
Fracture Mechanics

Linear elastic fracture mechanics (LEFM) requires that the amount of plasticity near the crack tip will be relatively small. As a "rule of thumb" LEFM can be considered to be valid if

$$r_p \leq 0.1 a$$

where r_p is the radius of the plastic zone around the crack tip and a is the crack length. Using Irwin's circular model for the plastic zone incorporating the upper bound dimension as obtained by a plane stress solution (see Fig. B.1),

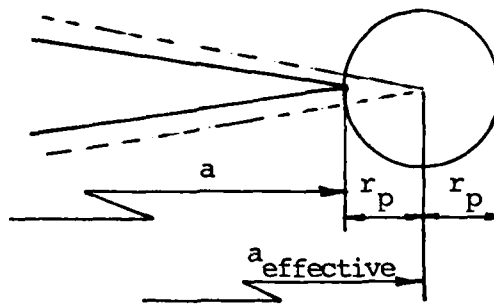


Fig. B.1. Irwin Circular Plastic Zone Model

$$r_p = \frac{1}{2\pi} \left(\frac{K_I}{\sigma_{y.s}} \right)^2 \quad (B-1)$$

where $\sigma_{y.s}$ is the yield strength of the material.

Using 7075 T651

$$\sigma_{y.s} = 80.8 \text{ ksi}$$

The maximum K_I used in our tests was lower than $15 \text{ ksi}\sqrt{\text{in.}}$.

Therefore, the maximum radius of plastic zone that has been developed was

$$r_p = \frac{1}{2\pi} \left(\frac{15}{80.8} \right)^2 = 0.0055 \text{ in}$$

The smallest crack length used was

$$a = 0.0815"$$

Thus,

$$\left(\frac{r_p}{a} \right)_{\max} = 0.0674 < 0.1$$

The conclusion is that LEFM was valid even in the most extreme conditions. In most cases the crack length was significantly longer and therefore r_p/a smaller.

Plane Stress/Strain Considerations

As a "rule of thumb" (Refs 15-16), if

$$b \geq 2.5 \left(\frac{K_{IC}}{\sigma_{y.s}} \right)^2 \quad (B-2)$$

where b is the material thickness, K_{IC} the fracture toughness, and $\sigma_{y.s}$ the yield strength.

The specimen can be considered thick enough to be under a plane strain stress field.

K_{IC} for 7075 T651 plate is $21.4 \text{ ksi}\sqrt{\text{in.}}$.

$$2.5 \left(\frac{K_{IC}}{\sigma_{y.s}} \right)^2 = 0.176"$$

Since .24"- .25" thick specimens were used, they can be viewed to be under plane strain conditions.

Appendix C

Laser Interferometer Data Reduction

A typical strip chart recorder trace of fringe motion crack mouth opening and load is shown in Fig. C.1. From this chart the fringe order versus load data can be obtained for the left and right fringe pattern as presented in Table C.1. The data can be plotted as shown in Fig. C2.

From Fig. C.2 slopes of $\delta m/P$ of the left and right fringe pattern can be obtained by considering only the linear part and ignoring the initial nonlinear part of the plot that is associated with fatigue crack closure effects. Those slopes are averaged to eliminate free body motion.

The experiment is repeated and results are averaged. The value of the slope is used in Eq (4-1) to get displacement per unit load data. Through Eq (4-2) stress intensity factors can be calculated.

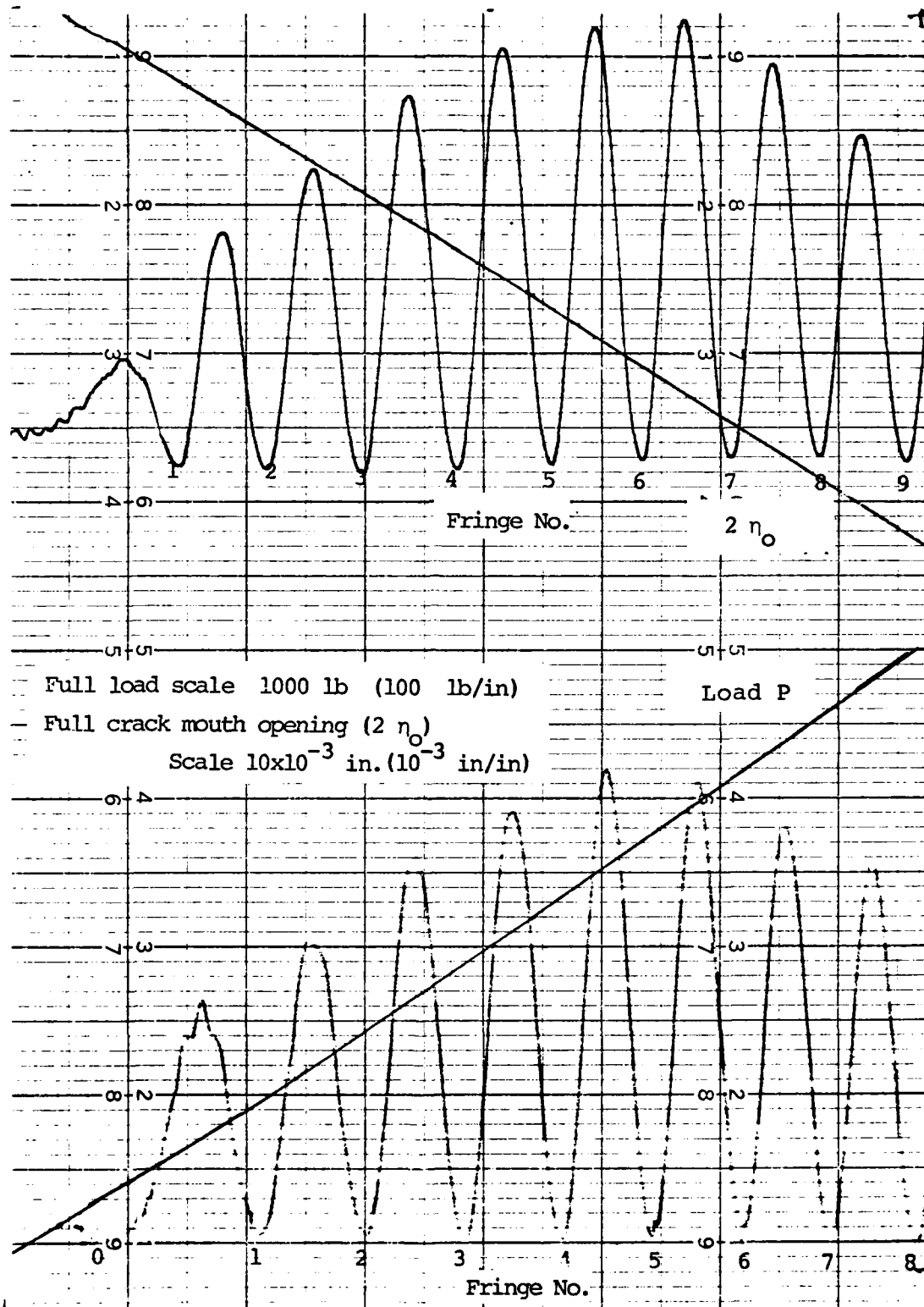


Fig. C.1. Typical Stripchart Recorder Trace of Fringe Motion, Load and Crack Mouth Opening

TABLE C.I

Fringe Order Versus Load

Fringe No.	Load Left Pattern	Load Right Pattern
0	120 lb.	60 lb.
1	190 lb.	150 lb.
2	237 lb.	190 lb.
3	278 lb.	235 lb.
4	320 lb.	275 lb.
5	365 lb.	320 lb.
6	410 lb.	360 lb.
7	450 lb.	400 lb.
8	490 lb.	445 lb.
9		485 lb.

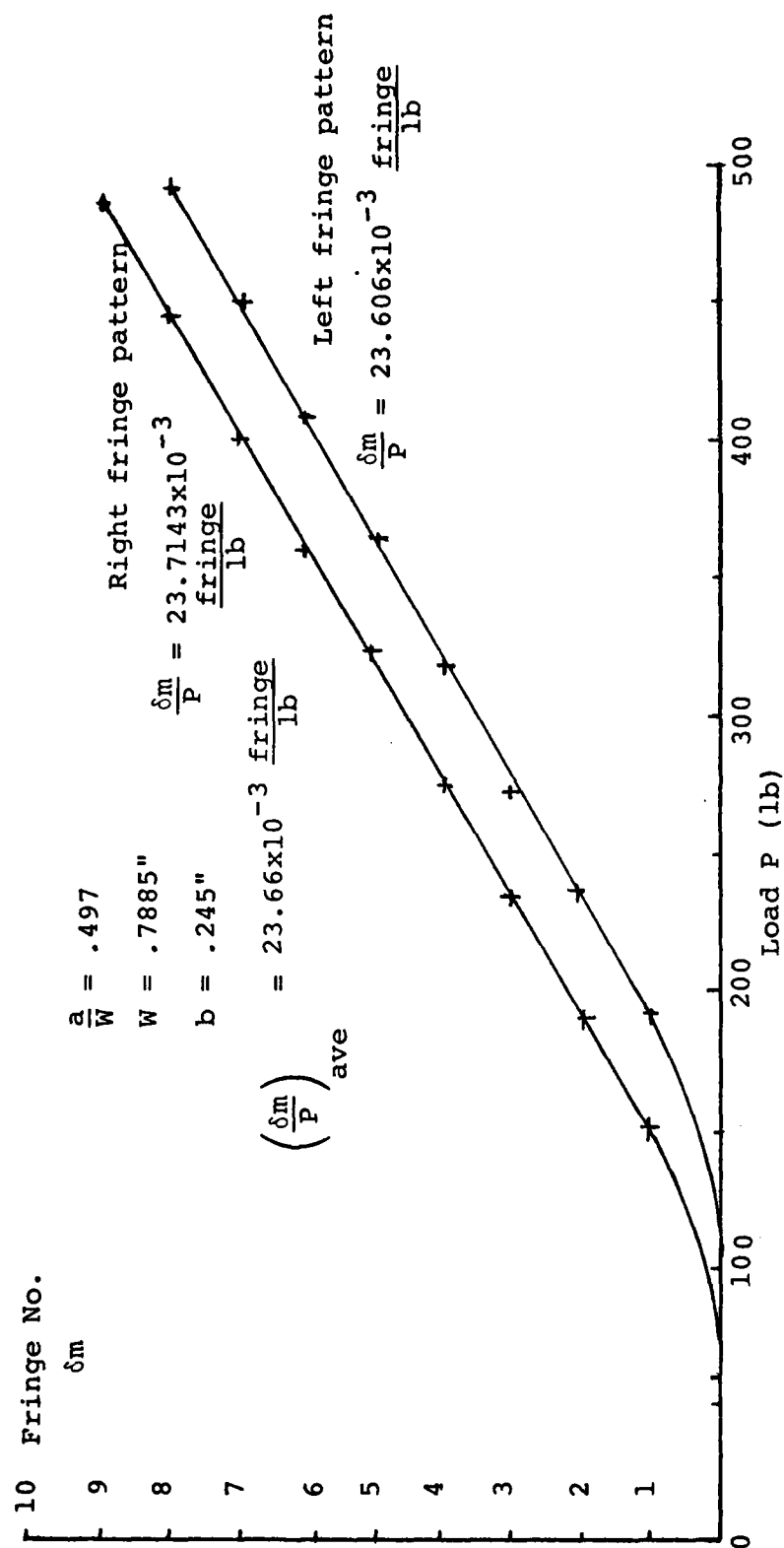


Fig. C.2. Typical Load-Fringe Motion Curve

Appendix D
Computer Program Description

The computer program has been written to perform the numerical computation involved in the process of data interpolation, weight function calculations and finally evaluation of the integral in Eq (2-30) to determine K_I for Case 2.

In order to allow maximum flexibility in the usage of the program it was constructed of a main program that performs the integration and nine subprograms that perform all the other necessary calculations. In addition, two library subprograms are used, one from the IMSL library and the other from the CC 6600 library. This structure of the program allows using it for different cases and configurations and permits the user to enter his own interpolation schemes, comparison functions and the noncracked body stress distribution $p(t)$ that makes it possible to compute any desired Case 2 stress intensity factor.

The program is written in FORTRAN and was executed on the CDC system at Wright-Patterson Air Force Base. Execution time for the three-point bending and uniform tension Case 2 stress intensity factor varied from two to four seconds.

The Main Program

The main program reads in the input data, calls in the different subroutines to perform necessary computation and performs the numeric integration by using the IMSL library subprogram DCADRE. An iterative scheme "pushes" down the lower integration limit until the desired accuracy for the end result is met. At the end, it prints out computed K_I for Case 2 compared to user-supplied comparison data.

Function Subprogram F(x)

This function computes the value of the integrant (the weight function multiplied by $P(t)$) at each distance t from the crack tip.

Function Subprogram P(x)

This function computes the value of the stress at the crack location $P(t)$ for a noncracked body at any distance t from the corresponding crack tip.

The function should be supplied by the user and is the only subprogram that has to be altered when computing K_I for different Case 2 configurations. Care should be taken as related to the form in which $P(t)$ is supplied. This form will determine the form of the calculated K_I . A factor of $1/\sqrt{\pi a}$ is already included in the weight function calculation. So if $P(t)$ is supplied directly in terms of stress, the resulting K_I values will be in the dimensional form of $K_I/\sqrt{\pi a}$.

Library Function PLSCF

A CC 6600 Library subroutine, computes least square polynomial fits for a given set of data. Polynomials up to 6 degrees or Chebyshev polynomials of any degree can be specified by the user. For further information see (Ref 25).

Library Function Subprogram DCADRE

An International Mathematics and Statistics IMSL Library subprogram. Performs numeric integration of a function using the Romberg extrapolation scheme. The function DCADRE is capable of integrating functions with "jump" discontinuities and certain types of singularity. This feature is most important in our case because of the crack tip singularity of the weight function. Even if the desired accuracy is not found, DCADRE returns the best available estimate. See IMSL Manual (Ref 26) for further information.

Subroutine KPOL

This subroutine computes a fourth order least square polynomial fit for the nondimensional K_I data using PLSCF subroutine from the CC 6600 library. It prints out the polynomial coefficients $C(5) \dots C(1)$ and returns these values to the main program. It also prints out the error flag IER from PLSCF.

Subroutine EPOL

This subroutine computes a fourth order least square polynomial fit for the nondimensional η_0 data using

PLSCF subroutine from the CC 6600 library. It prints out the polynomial coefficients $D(5), \dots, D(1)$ and returns them to the main program. It also prints out the error flag IER from PLSCF.

Subroutine EVEK

Evaluates the nondimensional K_I from the fourth order least square polynomial and the derivative of K_I with respect to crack length $\partial K_I / \partial a$ at the points where K_I for Case 2 should be evaluated. One should realize that the differentiation considers the fact that the nondimensional K_I usually factors out $1/\sqrt{a}$ that should be included in the differentiated term. The derivative $\partial K_I / \partial a$ requires the expression

$$\frac{\partial K_I}{\partial a} = \frac{\partial (\sigma \sqrt{\pi a} Y)}{\partial a} = \sigma \sqrt{\pi a} \left(\frac{Y}{2a} + \frac{\partial Y}{\partial a} \right)$$

where Y is the nondimensional K_I value and σ is the maximum tensile stress in the specimen. K_I and $\partial K_I / \partial a$ are returned to the main program in a dimensional form factored only by $1/\sigma$ as to match the η_0 data.

Subroutine EVETTA

Evaluates the nondimensional η_0 from the least square fourth order polynomial and the derivative of η_0 with respect to crack length $\partial \eta_0 / \partial a$, at the points where K_I for Case 2 should be evaluated. One should realize that the differentiation considers the fact that the

nondimensional η_0 is factored by a term of "a" that should be included in the differentiated term as applied in the above paragraph.

η_0 and $\partial\eta_0/\partial a$ are returned in a dimensional form factored by $1/\sigma$ to match the K_I data.

Subroutine COPK

Compares the nondimensional K_I input data with the interpolated data by KPOL at the test points. A comparison table that includes a relative error in percents is printed out for the user's evaluation and judgement.

Subroutine COPETA

Compares the nondimensional η_0 input data with interpolated data by EPOL at the test points. A comparison table that includes a relative error in percents is printed out for the user's evaluation and judgement.

Subroutine KANA

Evaluates K_I for the Case 2 loading configuration from a user-supplied comparison function. The evaluation is done at the same points where K_I Case 2 is evaluated from the experimental data. This subroutine can be eliminated if the above comparison data is available explicitly. In this case the comparison values should be assigned directly to AK array. If no comparison values are available, the final printout table should be altered to avoid undefined terms.

List of Symbols Used in the Program
(Alphabetical Order)

A	Constant used in subroutine KANA
AERR	Input, absolute error in the integral routine DCADRE
AK(99)	$K_{I(2)} / \sigma \sqrt{\pi a}$ comparison value of the K_I Case 2 nondimensional evaluated from the user-supplied comparison function at points defined by S
AKS(99)	$K_{I(2)} / \sigma \sqrt{\pi a}$ calculated values of K_I Case 2 (non- dimensional) at points defined by S
B	Interim term for weight function calculations
C(5)	Interpolating polynomial coefficients for K_I data
D(5)	Interpolating polynomial coefficients for η_o data
DB	Interim term for weight function calculation
DC	$\partial R / \partial a$ interim term for weight function calcu- lation
DY(99)	Interim derivative term for DYA
DYA(99)	$1/\sigma (\partial K_I / \partial a)$ derivative w.r.t the crack length of K_I Case 1 at points defined by S
D2(99)	Interim derivative term for DZA
DZA(99)	$1/\sigma (\partial \eta_o / \partial a)$ derivative w.r.t the crack length of η_o at points defined by S
EDS	Input, desired absolute accuracy in K_I computa- tion
ES(99)	$(AKS-AK)100/AK$ relative error in the computed K_I
EST	Current estimate of value of the integral by DCADRE
EY(99)	$(YC-Y)100/Y$ relative error in percents of interpolated K_I data at points defined by S

EZ(99)	(ZC-Z)100/Z relative error in percents of interpolated η_0 data at points defined by S
F	h, the weight function (subfunction)
G	Upper limit of the integral
H	Input, H material property
IER	Error flag for library subprograms PLSCF and DCADRE
M	Input, number of experimental data points
N	Input, number of points where K_I should be evaluated for Case 2
P	Stress distribution for the noncracked body at the crack location for Case 2 loading configuration (subfunction)
PI	π
Q	Lower limit of integral
R	Interim term for weight function calculation
RELERR	Input, relative error in the integration routine DCADRE
S(99)	Input, a/w, nondimensional crack length at point where experiments were performed
T	Interim term for weight function calculations
V	Previous interim value for EST
VA	(EST-V), difference between last and current integration estimate
W(99)	Weight corresponding to each data point used in PLSCF (currently defined as -1. to give equal weight to each point)
WORK(25)	Work array for PLSCF subroutine
X(99)	Input, a/w, nondimensional crack length for points where K_I Case 2 should be evaluated
Y(99)	Input, $K_I / \sigma \sqrt{\pi a}$, nondimensional K_I , experimental data

YA(99) K_I/σ , interpolated K_I for Case 1 at points defined by x

YC(99) $K_I/\sigma\sqrt{\pi a}$, interpolated nondimensional K_I for Case 1 at points defined by S

YK(99) $K_I/\sigma\sqrt{\pi a}$, interpolated nondimensional K_I for Case 1 at points defined by x

Z(99) Input, $\eta_o \cdot H/(2\sigma a)$, nondimensional crack mouth opening

ZA(99) η_o/σ , interpolated η_o at the points defined by x

ZC(99) $\eta_o H/(2\sigma a)$, interpolated nondimensional η_o at points defined by S

ZK(99) $\eta_o H/(2\sigma a)$, interpolated nondimensional η_o at points defined by x

Sequence of Input Data

Card Number	Variable	No. of Variables per card	Real/ Integer	Format
1	H	1	Real	Unformatted
2	AERR,RELERR,EPS	3	Real	Unformatted
3	M	1	Integer	Unformatted
3 to (M+3)	S(I),Y(I),Z(I)	3	Real	Unformatted
M+4	N	1	Integer	Unformatted
(M+5) to (M+N+5)	X(I)	1	Real	Unformatted

Sequence of Output Data

1. Interpolation polynomial coefficients for K_I
2. Interpolation polynomial coefficients for η_o
3. Comparison table of actual to interpolated K_I
4. Comparison table of actual to interpolated η_o

5. The following printout will appear only if singularities have been met by subroutine DCADRE. Each time a singularity was met a warning statement is printed out followed by the values of the crack length (X(I)) the distance from crack tip (Q) and the value of the error flag (IER) for which the singularity occurred. Values of IER equal to 65 or 66 indicate that the singularity was successfully handled. If any other value appears consult the IMSL Manual (Ref 26).

6. Comparison table of K_I for Case 2 calculated values and supplied comparison values.

Listing and Result Sample

The following pages include a complete listing of the program and a sample printout of results for uniform tension as Case 2 loading configuration.

79

```

119 PRINT*,"-----"
PRINT*," "
PRINT*," A/W - CRACK LENGTH RELATIVE TO WIDTH "
PRINT*," K-EXP - VALUES CALCULATED THROUGH THE WEIGH FUNCTION"
PRINT*," K-CAL - SUPPLIED COMPRESSION VALUES"
PRINT*," E - RELATIVE ERROR IN X"
PRINT*," "
PRINT*," A/W K-EXP K-CAL E"
PRINT*," "
DO 13 I=1,N
PRINT 10,X(I),AKS(I),AK(I),ES(I)
FORMAT(1X,1F6.4,1X,1F8.4,2X,1F8.4,2X,1F6.2)
CONTINUE
10 STOP"END OF PROGRAM"
13 END

```

```

1 FUNCTION F(X)
EXTERNAL P
COMMON/DAN/G,T,S,R,DB,DC
F=(T/2.)*((8*DB*X*DB*X**2+2.*R*X)/((9*X*R*R**2)+.5)*P(X)
RETURN
END

```

```

1 FUNCTION P(X)
COMMON/DAN/G,T,S,R,DB,DC
P=1.
RETURN
END

```



```

SUBROUTINE COPK(X,Y,C,M,YC,EY)
DIMENSION X(1),Y(1),C(F),YC(I),E(Y)
DO I=1,N
    Z=X(I)*M+C(M)+X(I)**2+Y(I)**2-C(2)*X(I)-C(1)*Y(I)
    PRINT *,Z
END DO
PRINT *," "
PRINT *," "
PRINT *,"COMPARISON OF ACTUAL DATA TO INTERPOLATED DATA"
PRINT *," "
PRINT *," A/M - CRACK LENGTH RELATIVE TO WIDTH - "
PRINT *," K-EXP ACTUAL DATA-"
PRINT *," K-CAL INTERPOLATED DATA"
PRINT *," E RELATIVE ERROR IN %"
PRINT *," "
PRINT *," A/M      K-EXP      K-CAL      E   "
PRINT *," "
DO J,I=1,N
    PRINT 3,X(I),Y(I),YC(I),E(I)
FORMAT(1X,IF6.0,X,IF8.0,Z,IF8.0,2X,IF6.0)
CONTINUE
RETURN
END
```

```

1  SUBROUTINE COPETA(X,Z,D,M,ZC,EZ)
2  DIMENSION X(1),Z(1),D(1),ZC(1),E(1)
3  DO 19 I=1,M
4  ZC(I)=D(I)*X(1)+4.0*(X(1)+Z(I))*Z(3)+(X(1)+2+D(2))*X(1)+0(1)
5  ZC(I)=(ZC(I)-Z(I))*100./Z(I)
6  PRINT*," "
7  PRINT*," "
8  PRINT*," "
9  PRINT*," "
10 PRINT*,"COMPERISON OF ACTUAL DATA TO INTERPOLATED DATA"
11 PRINT*," "
12 PRINT*," A/M = CRACK LENGTH RELATIVE TO WIDTH "
13 PRINT*," ETA-EXP ACTUAL DATA"
14 PRINT*," "
15 PRINT*," ETA-CAL INTERPOLATED DATA"
16 PRINT*," E
17 PRINT*," RELATIVE ERROR IN %"
18 PRINT*," "
19 PRINT*," A/M ETA-EXP ETA-CAL E "
20 PRINT*," "
21 DO 7 I=1,M
22 PRINT 9,X(I),Z(I),ZC(I),EZ(I)
23 FORMAT(1X,F6.4,X,F6.4,2H,1F9.0,2X,1F6.2)
24 CONTINUE
25 RETURN
26 END

```


PAGE 1

09/28/79 18.07.02

FTN 4.7+476

SUBROUTINE EVEETA 74/74 OPT=1

```

1      SUBROUTINE EVEETA(X,D,M,N,ZK,OZ4,ZA,DZ)
      DIMENSION X(1),D(5),ZK(1),OZ4(1),ZA(1),DZ(1)
      DO 5 I=1,N
      ZK(I)=O(5)*X(I)+O(4)*X(I)+O(3)*X(I)+O(2)*X(I)+O(1)
      ZA(I)=ZK(I)*2.*X(I)/H
      OZ4(I)=O(5)*X(I)+O(4)*X(I)+O(3)*X(I)+O(2)*X(I)+O(1)
      OZ4(I)= (2./H)*O(7(I))*Y(I)+ZK(I)
      RETURN
      END
5

```

PAGE 1

09/28/79 18.07.02

FTN 4.7+476

SUBROUTINE KANA 74/74 OPT=1

```

1      SUBROUTINE KANA(X,N,AK,PI)
      DIMENSION X(1),AK(1)
      DO 20 I=1,N
      A=X(1)*PI/2.
      AK(I)=((2.*TAN(A)/(PI*X(I)))+O(5))*((.752+2.02*X(I)+.37*1.-SIN(A)
      O(5)*3./COS(A))
      CONTINUE
      RETURN
      END
20

```

AD-A079 854

AIR FORCE INST OF TECH WRIGHT-PATTERSON AFB OH SCHOOL--ETC F/G 20/11
AN EXPERIMENTAL WEIGHT FUNCTION METHOD FOR STRESS INTENSITY FAC--ETC(U)
DEC 79 D BAR-TIKVA
AFIT/GAE/AA/79D-2

UNCLASSIFIED

NL

2 of 2

44 2096-4



END
DATE
FILMED
2-80

DDC



RESULTS

INTERPOLATION POLYNOMIAL FOR K

C(5)=76.75542913721
C(4)=-92.45527346502
C(3)=42.95455960156
C(2)=-6.52672584317
C(1)=1.25668785434

IER- ERROR FLAG-SEE ASD COMPUTER SUBPROGRAM LIBRARY GUIDE
IER=0

INTERPOLATION POLYNOMIAL FOR ETA

D(5)=210.3785059491
D(4)=-282.572732332
D(3)=150.7543040959
D(2)=-32.16174824038
D(1)=3.95288733928

IER- ERROR FLAG-SEE ASD COMPUTER SUBPROGRAM LIBRARY GUIDE
IER=0

COMPERISON OF ACTUAL DATA TO INTERPOLATED DATA

A/N - CRACK LENGTH RELATIVE TO WIDTH
K-EXP ACTUAL DATA
K-CAL INTERPOLATED DATA
E RELATIVE ERROR IN %

A/N	K-EXP	K-CAL	E
.1034	.9073	.9467	4.34
.1586	1.0575	.9776	-7.56
.2864	1.0572	1.0545	-.26
.2328	1.1137	1.1068	-.69
.2646	1.1087	1.1705	6.35
.2666	1.1862	1.1746	-.98
.3896	1.2366	1.2598	1.81
.3460	1.3498	1.3244	-1.82
.3978	1.3884	1.4086	2.84
.4368	1.4388	1.4696	2.14
.4768	1.4766	1.5424	-1.42
.4893	1.6551	1.5718	-5.08
.5788	1.8461	1.6774	-1.59
.6487	2.3468	2.3668	.97
.7517	3.4513	3.9413	-2.25

COMPARISON OF ACTUAL DATA TO INTERPOLATED DATA

A/N - CRACK LENGTH RELATIVE TO WIDTH
 ETA-EXP ACTUAL DATA
 ETA-CAL INTERPOLATED DATA
 E RELATIVE ERROR IN X

A/N	ETA-EXP	ETA-CAL	E
.1874	1.9448	1.9508	.31
.1906	1.6543	1.6491	-.91
.2004	1.6858	1.6334	-3.09
.2320	1.6163	1.6079	-.43
.2646	1.6098	1.7933	9.80
.2666	1.8796	1.8811	-.18
.3096	1.9981	1.9923	-.19
.3468	2.1688	2.1823	.75
.3978	2.6099	2.4945	-4.26
.4368	2.7493	2.7696	.74
.4768	3.0632	3.1251	2.02
.4893	3.2866	3.2648	-.66
.5780	4.5933	4.6431	1.08
.6467	5.6244	6.9725	23.78
.7517	12.0988	12.1862	.68

THE FOLLOWING PRINT OUT IS FROM THE NUMERICAL INTEGRATION
 SUBROUTINE(DCADRE) AND INDICATES THAT SINGULARITIES WERE
 HANDLED

ITER=65 FLAG=65 OR 66 -SINGULARITIES WERE SUCCESSFULLY HANDLED,ANY OTHER VALUE CONSULT INSL MANUAL
 X(1)=THE CRACK LENGTH FOR WHICH THE ERROR FLAG(ITER) APPLIES
 Q=DISTANCE FROM CRACK TIP RELATIVE TO WIDTH (T/W) FOR WHICH THE SINGULARITY WAS DETECTED

*** WARNING WITH FIX ERROR (IER = 65) FROM INSL ROUTINE DCADRE
 X(1)=.1
 Q=1.E-11
 IER=65
 *** WARNING WITH FIX ERROR (IER = 65) FROM INSL ROUTINE DCADRE
 X(1)=.1
 Q=1.E-12
 IER=65

*** WARNING WITH FIX ERROR (IER = 65) FROM INSL ROUTINE DCADRE
 X(2)=.45
 Q=1.E-18
 IER=65
 *** WARNING WITH FIX ERROR (IER = 65) FROM INSL ROUTINE DCADRE
 X(2)=.45
 Q=1.E-11
 IER=65
 *** WARNING WITH FIX ERROR (IER = 65) FROM INSL ROUTINE DCADRE
 X(2)=.15
 Q=1.E-12
 IER=65

*** WARNING WITH FIX ERROR (IER = 65) FROM INSL ROUTINE DCADRE
 X(3)=.2
 Q=1.E-18
 IER=65
 *** WARNING WITH FIX ERROR (IER = 65) FROM INSL ROUTINE DCADRE
 X(3)=.2
 Q=1.E-11
 IER=65
 *** WARNING WITH FIX ERROR (IER = 65) FROM INSL ROUTINE DCADRE
 X(3)=.2
 Q=1.E-12
 IER=65

*** WARNING WITH FIX ERROR (IER = 65) FROM INSL ROUTINE DCADRE
 X(4)=.25
 Q=1.E-18
 IER=65
 *** WARNING WITH FIX ERROR (IER = 65) FROM INSL ROUTINE DCADRE
 X(4)=.25
 Q=1.E-11
 IER=65
 *** WARNING WITH FIX ERROR (IER = 65) FROM INSL ROUTINE DCADRE
 X(4)=.25
 Q=1.E-12
 IER=65

*** WARNING WITH FIX ERROR (IER = 65) FROM INSL ROUTINE DCADRE
 X(5)=.3
 Q=1.E-9
 IER=65
 *** WARNING WITH FIX ERROR (IER = 65) FROM INSL ROUTINE DCADRE
 X(5)=.3
 Q=1.E-18
 IER=65
 *** WARNING WITH FIX ERROR (IER = 65) FROM INSL ROUTINE DCADRE
 X(5)=.3
 Q=1.E-11
 IER=65
 *** WARNING WITH FIX ERROR (IER = 65) FROM INSL ROUTINE DCADRE
 X(5)=.3
 Q=1.E-12
 IER=65

*** WARNING WITH FIX ERROR (IER = 65) FROM INSL ROUTINE DCADRE
 X(6)=.35
 Q=1.E-9
 IER=65
 *** WARNING WITH FIX ERROR (IER = 65) FROM INSL ROUTINE DCADRE
 X(6)=.35
 Q=1.E-18
 IER=65
 *** WARNING WITH FIX ERROR (IER = 65) FROM INSL ROUTINE DCADRE
 X(6)=.35
 Q=1.E-11
 IER=65
 *** WARNING WITH FIX ERROR (IER = 65) FROM INSL ROUTINE DCADRE
 X(6)=.35
 Q=1.E-12
 IER=65

```

*** WARNING WITH FIX ERROR (IER = 65) FROM INSL ROUTINE DCADRE
X(17)=.4
Q=1.E-9
IER=65
*** WARNING WITH FIX ERROR (IER = 65) FROM INSL ROUTINE DCADRE
X(17)=.4
Q=1.E-10
IER=65
*** WARNING WITH FIX ERROR (IER = 65) FROM INSL ROUTINE DCADRE
X(17)=.4
Q=1.E-11
IER=65
*** WARNING WITH FIX ERROR (IER = 65) FROM INSL ROUTINE DCADRE
X(17)=.4
Q=1.E-12
IER=65

*** WARNING WITH FIX ERROR (IER = 65) FROM INSL ROUTINE DCADRE
X(1)=.45
Q=1.E-9
IER=65
*** WARNING WITH FIX ERROR (IER = 65) FROM INSL ROUTINE DCADRE
X(1)=.45
Q=1.E-10
IER=65
*** WARNING WITH FIX ERROR (IER = 65) FROM INSL ROUTINE DCADRE
X(1)=.45
Q=1.E-11
IER=65

*** WARNING WITH FIX ERROR (IER = 65) FROM INSL ROUTINE DCADRE
X(9)=.5
Q=1.E-9
IER=65
*** WARNING WITH FIX ERROR (IER = 65) FROM INSL ROUTINE DCADRE
X(9)=.5
Q=1.E-10
IER=65
*** WARNING WITH FIX ERROR (IER = 65) FROM INSL ROUTINE DCADRE
X(9)=.5
Q=1.E-11
IER=65

*** WARNING WITH FIX ERROR (IER = 65) FROM INSL ROUTINE DCADRE
X(18)=.55
Q=1.E-9
IER=65
*** WARNING WITH FIX ERROR (IER = 65) FROM INSL ROUTINE DCADRE
X(18)=.55
Q=1.E-10
IER=65
*** WARNING WITH FIX ERROR (IER = 65) FROM INSL ROUTINE DCADRE
X(18)=.55
Q=1.E-11
IER=65

*** WARNING WITH FIX ERROR (IER = 65) FROM INSL ROUTINE DCADRE
X(11)=.6
Q=1.E-9
IER=65
*** WARNING WITH FIX ERROR (IER = 65) FROM INSL ROUTINE DCADRE
X(11)=.6

```

```

...
IER=65
*** WARNING WITH FIX ERROR (IER = 65) FROM INSL ROUTINE DCADRE
X(11)=.6
Q=1.E-11
IER=65

```

```

*** WARNING WITH FIX ERROR (IER = 65) FROM INSL ROUTINE DCADRE
X(12)=.65
Q=1.E-8
IER=65
*** WARNING WITH FIX ERROR (IER = 65) FROM INSL ROUTINE DCADRE
X(12)=.65
Q=1.E-9
IER=65
*** WARNING WITH FIX ERROR (IER = 65) FROM INSL ROUTINE DCADRE
X(12)=.65
Q=1.E-10
IER=65
*** WARNING WITH FIX ERROR (IER = 65) FROM INSL ROUTINE DCADRE
X(12)=.65
Q=1.E-11
IER=65

```

```

*** WARNING WITH FIX ERROR (IER = 66) FROM INSL ROUTINE DCADRE
X(13)=.7
Q=1.E-7
IER=66
*** WARNING WITH FIX ERROR (IER = 66) FROM INSL ROUTINE DCADRE
X(13)=.7
Q=1.E-8
IER=66
*** WARNING WITH FIX ERROR (IER = 66) FROM INSL ROUTINE DCADRE
X(13)=.7
Q=1.E-9
IER=66
*** WARNING WITH FIX ERROR (IER = 66) FROM INSL ROUTINE DCADRE
X(13)=.7
Q=1.E-10
IER=66
*** WARNING WITH FIX ERROR (IER = 66) FROM INSL ROUTINE DCADRE
X(13)=.7
Q=1.E-11
IER=66

```

```

*** WARNING WITH FIX ERROR (IER = 65) FROM INSL ROUTINE DCADRE
X(14)=.75
Q=1.E-8
IER=65
*** WARNING WITH FIX ERROR (IER = 65) FROM INSL ROUTINE DCADRE
X(14)=.75
Q=1.E-9
IER=65
*** WARNING WITH FIX ERROR (IER = 65) FROM INSL ROUTINE DCADRE
X(14)=.75
Q=1.E-10
IER=65
*** WARNING WITH FIX ERROR (IER = 65) FROM INSL ROUTINE DCADRE
X(14)=.75
Q=1.E-11
IER=65

```

```

*****
X(15)=.8
O-1.E-7
IER=66
*** WARNING WITH FIX ERROR (IER = 66) FROM INSL ROUTINE DCADRE
X(15)=.8
O-1.E-8
IER=66
*** WARNING WITH FIX ERROR (IER = 66) FROM INSL ROUTINE DCADRE
X(15)=.8
O-1.E-9
IER=66
*** WARNING WITH FIX ERROR (IER = 66) FROM INSL ROUTINE DCADRE
X(15)=.8
O-1.E-10
IER=66
*** WARNING WITH FIX ERROR (IER = 66) FROM INSL ROUTINE DCADRE
X(15)=.8
O-1.E-11
IER=66
*** WARNING WITH FIX ERROR (IER = 66) FROM INSL ROUTINE DCADRE
X(15)=.8
O-1.E-12
IER=66
*** WARNING WITH FIX ERROR (IER = 66) FROM INSL ROUTINE DCADRE

```

RESULTS FOR K UNIFORM TENSION USING THE WEIGHT FUNCTION METHOD(K-NON DIMENSIONAL)

A/W - CRACK LENGTH RELATIVE TO WIDTH
K-EXP - VALUES CALCULATED THROUGH THE WEIGH FUNCTION
K-CAL - SUPPLIED COMPERISON VALUES
E - RELATIVE ERROR IN %

A/W	K-EXP	K-CAL	E
.1000	1.2785	1.1957	6.26
.1500	1.2697	1.2682	.12
.2000	1.4061	1.3667	2.74
.2500	1.5548	1.4941	4.01
.3000	1.6895	1.6551	1.83
.3500	1.8178	1.8565	-2.13
.4000	1.9367	2.1080	-9.20
.4500	2.2917	2.4241	-5.46
.5000	2.7719	2.8266	-1.93
.5500	3.4752	3.3486	3.78
.6000	4.3636	4.8432	-10.92
.6500	5.3158	4.9993	6.33
.7000	6.4832	6.3755	1.92
.7500	8.0662	8.4889	-5.84
.8000	10.3400	11.9926	-30.79

Appendix E

Crack Shape--Conical Approximation

Following Orange (Ref 11), the shape of a crack can be approximated by a conic section equation. Requiring that the crack opening at the crack mouth will match the actual crack mouth opening η_o one can write a general form for the conic section; equation;

$$\left(\frac{\eta}{\eta_o}\right)^2 = \frac{2}{(2+\bar{m})} \left(\frac{t}{a}\right) + \frac{\bar{m}}{2+\bar{m}} \left(\frac{t}{a}\right)^2 \quad (E-1)$$

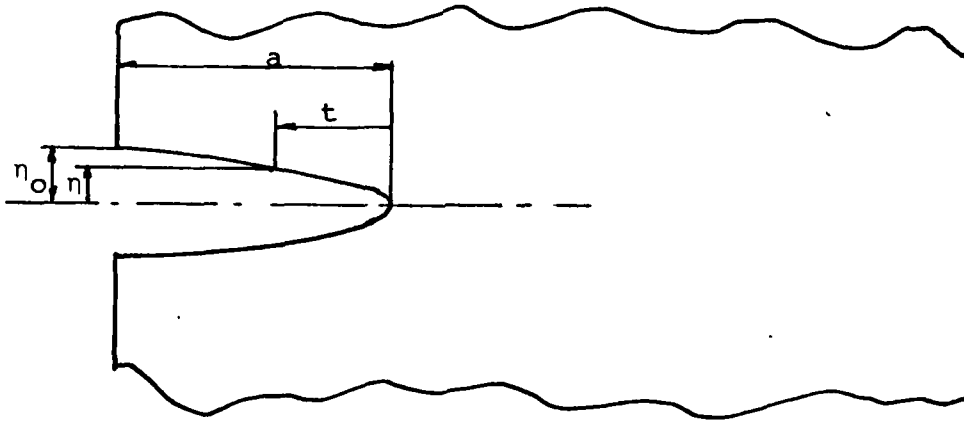


Fig. E.1. Crack Opening Conical Approximation

where t is the distance from the crack tip, a is the crack length, and \bar{m} is the conic section coefficient to be determined. The type of conical section depends on \bar{m} if

- $\bar{m} < 0$ - ellipse
- $\bar{m} = 0$ - parabola
- $0 < \bar{m} < \infty$ - hyperbola
- $\bar{m} = \infty$ - a pair of straight lines

In order to determine the unknown conic section coefficient \bar{m} , let's match the radius of curvature at the crack tip from the Eq (E-1) to the curvature resulting from the crack tip displacement field as expressed in Eq (2-16).

Using the following definition for the curvature of a two-dimensional curve defined by

$$y = f(x) \quad (E-2)$$

the curvature \bar{K} is given by

$$K = \frac{-\frac{d^2x}{dy^2}}{\left\{ 1 + \left(\frac{dx}{dy} \right)^2 \right\}^{\frac{3}{2}}} \quad (E-3)$$

and the radius of curvature is

$$\bar{R} = \left[\frac{1}{\bar{K}} \right] \quad (E-4)$$

provided $\bar{K} \neq 0$

If one uses the near crack tip displacement field from Eq (2-16)

$$t = \frac{\pi H^2}{8K_I} \eta^2 \quad (E-5)$$

$$\frac{\partial t}{\partial \eta} = \frac{\pi H^2}{4K_I} \eta \quad (E-6)$$

and at the crack tip

$$\eta = 0$$

$$t = 0.$$

$$\text{From Eq E-6)} \quad \left. \frac{\partial t}{\partial \eta} \right|_{\eta=0} = 0 \quad (E-7)$$

Also from Eq (E-6)

$$\frac{\partial^2 t}{\partial \eta^2} = \frac{\pi H^2}{4K_I} \quad (E-8)$$

Substituting Eqs (E-7, E-8) into Eq (E-3) and then using Eq (E-4), the radius of curvature at the crack tip from the crack tip displacement field is

$$\bar{R} = \frac{4K_I^2}{\pi H^2} \quad (E-9)$$

Now find the radius of curvature from the conic section Eq (E-1)

$$\eta^2 = \frac{2\eta_o^2}{(2+\bar{m})a} t + \frac{\bar{m}\eta_o^2}{(2+\bar{m})a^2} t^2 \quad (E-10)$$

Differentiate twice with respect to η

$$2\eta = \frac{2\eta_o}{(2+\bar{m})a} \frac{\partial t}{\partial \eta} + \frac{2\bar{m}\eta_o^2}{(2+\bar{m})a^2} t \cdot \frac{\partial t}{\partial \eta} \quad (\text{E-11})$$

$$2 = \frac{2\eta_o^2}{(2+\bar{m})a} \frac{\partial^2 t}{\partial \eta^2} + \frac{2\bar{m}\eta_o^2}{(2+\bar{m})a^2} \left[\left(\frac{\partial t}{\partial \eta} \right)^2 + t \frac{\partial^2 t}{\partial \eta^2} \right] \quad (\text{E-12})$$

From Eqs (E-11, E-12) at the crack tip

$$t=0, \quad \eta=0$$

The value

$$\frac{\partial t}{\partial \eta} = 0$$

and

$$\frac{\partial^2 t}{\partial \eta^2} = \frac{(2+\bar{m})a}{\eta_o^2} \quad (\text{E-13})$$

If Eqs (E-3, E-4) are used, the radius of curvature at the tip of the conic section is

$$R = \frac{\eta_o^2}{(\bar{m}+2)a} \quad (\text{E-14})$$

Now, matching the radius of curvature at the crack tip of the conic section (Eq E-14) to the one that is derived from the crack tip displacement field Eq (E-9), one can determine the conic section coefficient

$$\bar{m} = \pi \left(\frac{\eta_o H}{2K_I \sqrt{a}} \right)^2 - 2 \quad (\text{E-14})$$

Thus, following Orange and substituting the stress intensity factor K_I , with the nondimensional stress intensity factor Y defined by the relation

$$K_I = Y\sigma\sqrt{a}$$

The value of \bar{m} becomes;

$$\bar{m} = \pi \left[\frac{\eta_o H}{2Y\sigma a} \right]^2 - 2 \quad (E-15)$$

where

$$Y = \frac{K}{\sigma\sqrt{a}} \quad (E-16)$$

Vita

Dan Bar-Tikva was born on 8 October 1948 in Tel-Aviv, Israel. He was graduated from Tichon Ironi Alef high school in Tel-Aviv in 1966. He studied in the Technician, Israeli Institution of Technology through the ROTC program and was awarded a Bachelor of Science degree in Aeronautical Engineering in 1970. He joined the Israeli Air Force in November 1970 and went through various assignments until he was selected to join the graduate program at AFIT in June 1978. He is married to the former Rachel Greenfeld, and they have two sons, Amir and Ran.

PERMANENT ADDRESS: 17 Neve Reim Street
Petach-Tiqua, Israel

UNCLASSIFIED

SECURITY CLASSIFICATION OF THIS PAGE (When Data Entered)

REPORT DOCUMENTATION PAGE		READ INSTRUCTIONS BEFORE COMPLETING FORM
1. REPORT NUMBER AFIT/GAE/AA/79D-2	2. GOVT ACCESSION NO.	3. RECIPIENT'S CATALOG NUMBER
4. TITLE (and Subtitle) AN EXPERIMENTAL WEIGHT FUNCTION METHOD FOR STRESS INTENSITY FACTOR CALIBRATION		5. TYPE OF REPORT & PERIOD COVERED MS Thesis
		6. PERFORMING ORG. REPORT NUMBER
7. AUTHOR(s) Dan Bar-Tikva Major, IAF		8. CONTRACT OR GRANT NUMBER(s)
9. PERFORMING ORGANIZATION NAME AND ADDRESS Air Force Institute of Technology (AFIT/EN) Wright-Patterson AFB, Ohio 45433		10. PROGRAM ELEMENT, PROJECT, TASK AREA & WORK UNIT NUMBERS
11. CONTROLLING OFFICE NAME AND ADDRESS		12. REPORT DATE December 1979
		13. NUMBER OF PAGES 95
14. MONITORING AGENCY NAME & ADDRESS (if different from Controlling Office)		15. SECURITY CLASS. (of this report) UNCLASSIFIED
		15a. DECLASSIFICATION/DOWNGRADING SCHEDULE
16. DISTRIBUTION STATEMENT (of this Report) Approved for public release; distribution unlimited; IAW AFR 190-17 JOSEPH P. HIPPS, Major, USAF Director of Office of Public Affairs		
17. DISTRIBUTION STATEMENT (of the abstract entered in Block 20, if different from Report)		
18. SUPPLEMENTARY NOTES		
19. KEY WORDS (Continue on reverse side if necessary and identify by block number) Stress Intensity Factor Weight Function Crack Opening		
20. ABSTRACT (Continue on reverse side if necessary and identify by block number) The weight function procedure allows one to convert stress intensity factors K and crack displacement information obtained for one crack configuration and loading into the stress intensity factor solution for the same geometry and another loading. The feasibility of using the weight function idea for a two-dimensional case with experimental results is demonstrated in this work. Mode I stress intensity factor K_I measurements →		

DD FORM 1 JAN 73 1473

EDITION OF 1 NOV 65 IS OBSOLETE

UNCLASSIFIED

SECURITY CLASSIFICATION OF THIS PAGE (When Data Entered)

UNCLASSIFIED

SECURITY CLASSIFICATION OF THIS PAGE(When Data Entered)

obtained by a laser interferometric technique, and "crack mouth" opening displacement measurements were taken for an edge cracked strip subjected to four point bending. These results were used to construct (numerically) a weight function with the aid of a computer program written for this purpose.

Results of K_f for the same geometry with two different loading configurations, uniform tension and three point bending (with two different length to width ratios) were computed.

These results agree favorably with the known solutions and demonstrate that a set of experiments for a single loading can accurately predict the stress intensity factor for any other loading configuration of the same geometry. The advantage of the weight function method would be particularly important if these loading configurations are difficult or impossible to reproduce in the laboratory.

UNCLASSIFIED

SECURITY CLASSIFICATION OF THIS PAGE(When Data Entered)